Journal of Computational and Applied Mathematics 320 (2017) 43–60

Contents lists available at ScienceDirect

Journal of Computational and Applied Mathematics

journal homepage: www.elsevier.com/locate/cam

Numerical analysis of a characteristic stabilized finite element method for the time-dependent Navier–Stokes equations with nonlinear slip boundary conditions☆

Feifei Jing [a], Jian Li [b,c], Zhangxin Chen [a,d,*], Zhonghua Zhang [e]

[a] College of Mathematics and Statistics, Center for Computational Geoscience, Xi'an Jiaotong University, Xi'an 710049, PR China
[b] Department of Mathematics, School of Arts and Sciences, Shaanxi University of Science and Technology, Xi'an 710021, PR China
[c] Institute of Computational Mathematics and its Applications, Baoji University of Arts and Sciences, Baoji 721013, PR China
[d] Department of Chemical and Petroleum Engineering, Schulich School of Engineering, University of Calgary, 2500 University Drive N. W. Calgary, Alberta, T2N 1N4, Canada
[e] School of Sciences, Xi'an University of Science and Technology, Xi'an 710054, PR China

ARTICLE INFO

Article history:
Received 18 April 2015
Received in revised form 15 December 2016

Keywords:
Time-dependent Navier–Stokes equations
Nonlinear slip boundary conditions
Characteristic method
Lower order finite element pairs
Error estimates

ABSTRACT

Based on a characteristic method, this work is concerned with a finite element approximation to the time-dependent Navier–Stokes equations with nonlinear slip boundary conditions. Since this slip boundary condition of friction type contains a subdifferential property, its continuous variational problem is formulated as an inequality, which can turn into an equality problem by using a powerful regularized method. Then a fully discrete characteristic scheme under the stabilized lower order finite element pairs is proposed for the equality problem. Optimal error estimates for velocity and pressure are derived under the corresponding L^2, H^1-norms. Finally, a smooth problem test is reported to demonstrate the theoretically predicted convergence order and the expected slip phenomena, and the simulation of a bifurcated blood flow model is displayed to illustrate the efficiency of the proposed method.

1. Introduction

In this paper, we will consider the mathematical model of viscous incompressible fluid, which can be written as the following time-dependent Navier–Stokes equations

$$\begin{cases} \dfrac{\partial \boldsymbol{u}}{\partial t} - \nu \Delta \boldsymbol{u} + (\boldsymbol{u}\cdot\nabla)\boldsymbol{u} + \nabla p = \boldsymbol{f} & \text{in} \quad \Omega \times J, \\ \operatorname{div} \boldsymbol{u} = 0 & \text{in} \quad \Omega \times J, \\ \boldsymbol{u}(0) = \boldsymbol{u}_0 & \text{in} \quad \Omega \times \{0\}, \end{cases} \tag{1.1}$$

where $J = (0, T]$ $(0 < T < \infty)$ is a given time interval, $\Omega \subset \mathbb{R}^2$ is a bounded convex domain with a Lipschitz continuous boundary $\Gamma = \partial\Omega$, $\boldsymbol{u}(x, t)$ and $\boldsymbol{f}(x, t)$ denote the flow velocity and the external force, $p(x, t)$ is pressure, and $\nu > 0$ is the

☆ This work is supported by the National Natural Sciences Foundation of China (Nos. 11371031, and 11371288), partially supported by Foundation CMG in Xi'an Jiaotong University, Natural Science Basic Research Plan in Shaanxi Province of China (No. 2015JM1011).

* Corresponding author at: Department of Chemical and Petroleum Engineering, Schulich School of Engineering, University of Calgary, 2500 University Drive N. W. Calgary, Alberta, T2N 1N4, Canada.
E-mail addresses: jingfei.cool@163.com (F. Jing), jiaaanli@gmail.com (J. Li), zhachen@ucalgary.ca (Z. Chen), wwwzhonghua@sohu.com (Z. Zhang).

http://dx.doi.org/10.1016/j.cam.2017.01.012
0377-0427/

kinematic viscosity. Moreover, the boundary conditions are presented as follows:

$$\begin{cases} \boldsymbol{u} = 0 & \text{on} \quad \Gamma_D, \\ u_{\boldsymbol{n}} = 0, \quad |\boldsymbol{\sigma}_{\boldsymbol{\tau}}| \le g, & \boldsymbol{\sigma}_{\boldsymbol{\tau}} \boldsymbol{u}_{\boldsymbol{\tau}} + g|\boldsymbol{u}_{\boldsymbol{\tau}}| = 0 \quad \text{on} \quad \Gamma_S, \end{cases} \tag{1.2}$$

where $\Gamma = \overline{\Gamma}_D \cup \overline{\Gamma}_S$. The adhesive Dirichlet boundary condition is imposed on Γ_D, and for Γ_S, a nonlinear slip and non-leak boundary conditions are considered. Assume that both Γ_S and Γ_D are not empty and $\Gamma_D \cap \Gamma_S = \emptyset$. Here and what follows, the unit outward normal vector and the tangent vector to the boundary are denoted by $\boldsymbol{n}$ and $\boldsymbol{\tau}$, respectively. For a vector field $\boldsymbol{v}$ on the boundary, $\boldsymbol{v} \cdot \boldsymbol{n}$ and $\boldsymbol{v} \cdot \boldsymbol{\tau}$ are its normal and tangential components. Let $v_{\boldsymbol{n}} \equiv \boldsymbol{v} \cdot \boldsymbol{n}$ and $\boldsymbol{v}_{\boldsymbol{\tau}} \equiv \boldsymbol{v} - v_{\boldsymbol{n}} \boldsymbol{n}$. Denote by $\boldsymbol{\sigma}_{\boldsymbol{\tau}}(\boldsymbol{u}) = \nu \frac{\partial \boldsymbol{u}_{\boldsymbol{\tau}}}{\partial \boldsymbol{n}}$, independent of p, the tangential component of stress vector defined on Γ_S. The frictional function g, is assumed to be continuous on $\overline{\Gamma}_S$ and strictly positive on Γ_S. This friction type of boundary conditions was first introduced by Fujita in [1] and appeared in the modeling of blood flow in a vein of an arterial sclerosis patient and some other models.

For such boundary conditions (1.2), Fujita in [2] showed existence and uniqueness of a weak solution for the Stokes problem. From a theoretical point, some well-posedness analyses for the Stokes problem with nonlinear slip boundary conditions have been discussed during the past years [3–6]. In addition, numerical results for the steady Stokes and Navier–Stokes problems with such boundary conditions can be found in [7–12]. However, to our knowledge, there has not been much work on an analysis of finite element (FE) approximations to the unsteady problems with such boundary conditions. Djoko in [13] considered a semi-discrete scheme in time for the unsteady Stokes variational inequality problem by means of a regularized method, Kashiwabara in [14] investigated the weak solutions of the continuous variational inequality problem governed by the non-stationary Navier–Stokes equations, Li in [15] used the regularized method to obtain existence, uniqueness and regularity of global weak solutions to the two-dimensional time-dependent Navier–Stokes equations with nonlinear slip boundary conditions, and also stabilized FE methods are employed to solve this problem in [16], where the following convergence estimates with respect to a regularization parameter ε are established:

$$\begin{cases} \|\boldsymbol{u} - \boldsymbol{u}^{\varepsilon}\|_{L^\infty(0,T;\boldsymbol{L}^2)} \le C\varepsilon^{\frac{1}{2}}, \\ \|\boldsymbol{u} - \boldsymbol{u}^{\varepsilon}\|_{L^2(0,T;\boldsymbol{H}^1)} + \|p - p^{\varepsilon}\|_{L^2(0,T;L^2)} \le C\varepsilon^{\frac{1}{2}}, \end{cases}$$

where $(\boldsymbol{u}, p)$ and $(\boldsymbol{u}^{\varepsilon}, p^{\varepsilon})$ are the solutions of the Navier–Stokes type variational inequality problem and its regularized problem, respectively, and the constant $C > 0$ is independent of ε.

Since the characteristic methods can effectively weaken a non-physical phenomenon caused by nonlinear term $(\boldsymbol{u} \cdot \nabla)\boldsymbol{u}$ [17,18], which via rewriting the governing equations (1.1) in terms of Lagrangian coordinates defined by the particle trajectories associated with the problem under consideration [19]. The Lagrangian treatment can greatly reduce a time truncation error in the Eulerian method [20], and the characteristic methods have been shown to possess remarkable stability properties [21,22]. Furthermore, it is well-known that a regularized method plays a key role in theoretical and numerical analysis of a variational inequality problem, which turns the variational inequality into equations. In this work, with the help of regularized technology, we combine the characteristic method with the pressure projection stabilized method to solve the time-dependent Navier–Stokes problem with nonlinear slip boundary conditions, and we derive the optimal error estimates based on the following FE approximation:

$$\begin{cases} \|\boldsymbol{u}^{\varepsilon}(t_m) - \boldsymbol{u}_h^{\varepsilon}(t_m)\|_{H^1} + \|p^{\varepsilon}(t_m) - p_h^{\varepsilon}(t_m)\|_{L^2} \le Ch, \\ \|\boldsymbol{u}^{\varepsilon}(t_m) - \boldsymbol{u}_h^{\varepsilon}(t_m)\|_{L^2} \le Ch^2. \end{cases}$$

The organization of this paper is given as follows. In the next section, we will introduce some function spaces, existence of weak solutions of the discussed problem, the characteristic method and the corresponding regularized problem. In Section 3, we will develop a first-order fully discrete scheme of the characteristic regularized continuous equality problem. Our analysis shows that this fully discrete scheme is unconditionally stable provided that the characteristics are transported by a divergence-free velocity field. Optimal error estimates for the characteristic stabilized method are derived in Section 4. This work ends with a section of numerical examples. Slip and non-slip phenomena are shown that depend on the friction function, the obtained optimal error estimates are consistent with theoretical analysis, results of the blood flow model further illustrate the feasibility of the proposed method.

2. Statement of the Navier–Stokes equations with nonlinear slip boundary conditions

2.1. Weak form of the problem

Let $H_0^1(\Omega)$ be the standard Sobolev space [23] equipped with the usual norm $\|\cdot\|_1$. For function spaces corresponding to velocity and pressure, we introduce closed subspaces of $[H^1(\Omega)]^2$ or $L^2(\Omega)$ as follows:

$$\boldsymbol{V} = \{\boldsymbol{v} \in [H^1(\Omega)]^2 : \boldsymbol{v}|_{\Gamma_D} = 0, v_{\boldsymbol{n}}|_{\Gamma_S} = 0\}, \boldsymbol{V}_o = \{\boldsymbol{v} \in \boldsymbol{V} : \operatorname{div} \boldsymbol{v} = 0\}, \boldsymbol{Y} = \boldsymbol{L}^2(\Omega), \overset{\circ}{\boldsymbol{V}} = [H_0^1(\Omega)]^2,$$

$$Q = L_0^2(\Omega) = \left\{ q \in L^2(\Omega), \int_\Omega q \, \mathrm{d}\boldsymbol{x} = 0 \right\}, \boldsymbol{H} = \{\boldsymbol{v} \in L^2(\Omega)^2 | \operatorname{div} \boldsymbol{v} = 0 \text{ in } \Omega \text{ and } v_{\boldsymbol{n}} = 0 \text{ on } \partial\Omega\}.$$

The scalar product and norm in Q are denoted by the usual $L^2(\Omega)$ inner product and $\|\cdot\|_0$. $(\nabla\cdot, \nabla\cdot)$ and $\|\nabla\cdot\|_0 = \|\cdot\|_{\boldsymbol{V}}$ are the inner product and norm in $\boldsymbol{V}$, respectively. We denote by $C^{0,1}(\overline{\Omega})$ the space of Lipschitz continuous functions on the closure of Ω. The spaces consisting of vector-valued functions are denoted in boldface. Moreover, the symbol C denotes a generic positive constant whose value may change at different locations.

If X is a Banach space normed by $\|\cdot\|_X$, we define

$$L^p(0,T;X) = \left\{ v : [0,T] \to X \mid \int_0^T \|v(t)\|_X^p \,\mathrm{d}t < \infty \right\} \quad 1 \le p < \infty,$$

$$L^\infty(0,T;X) = \left\{ v : [0,T] \to X \mid \sup_{t\in[0,T]} \|v(t)\|_X \,\mathrm{d}t < \infty \right\},$$

and let M be a positive integer, $\triangle t = T/M$, $t_m = m\triangle t$, then

$$l^p(0,T;X) = \left\{ v : \{t_1,\ldots,t_M\} \longrightarrow X \mid \|v\|_{l^p(0,T;X)} = \left[\triangle t \sum_{i=1}^{M} \|v(t_i)\|_X^p \right]^{\frac{1}{p}} < \infty \right\} \quad 1 \le p < \infty,$$

$$l^\infty(0,T;X) = \left\{ v : \{t_1,\ldots,t_M\} \longrightarrow X \mid \|v\|_{l^\infty(0,T;X)} = \max_{1\le i<M} \|v(t_i)\|_X < \infty \right\}.$$

The continuous bilinear forms $a(\cdot,\cdot)$ and $d(\cdot,\cdot)$ on $\boldsymbol{V}\times\boldsymbol{V}$ and $\boldsymbol{V}\times Q$ are given as follows:

$$a(\boldsymbol{u},\boldsymbol{v}) = \nu(\nabla\boldsymbol{u},\nabla\boldsymbol{v}),\ \ d(\boldsymbol{v},p) = (\operatorname{div}\boldsymbol{v},p) \quad \forall\boldsymbol{u},\boldsymbol{v}\in\boldsymbol{V},\ \ \forall p\in Q.$$

If $\operatorname{div}\boldsymbol{u} = 0$, the trilinear form $b(\cdot;\cdot,\cdot)$ satisfies

$$b(\boldsymbol{u};\boldsymbol{v},\boldsymbol{w}) = ((\boldsymbol{u}\cdot\nabla)\boldsymbol{v},\boldsymbol{w}) + \frac{1}{2}((\operatorname{div}\boldsymbol{u})\boldsymbol{v},\boldsymbol{w}) = \frac{1}{2}((\boldsymbol{u}\cdot\nabla)\boldsymbol{v},\boldsymbol{w}) - \frac{1}{2}((\boldsymbol{u}\cdot\nabla)\boldsymbol{w},\boldsymbol{v}) \quad \forall\,\boldsymbol{u}\in\boldsymbol{V}_o,\ \boldsymbol{v},\boldsymbol{w}\in\boldsymbol{V}.$$

Given $\boldsymbol{u}_0\in\boldsymbol{H}, \boldsymbol{f}\in L^2(0,T;\boldsymbol{Y})$, and $g\in L^2(0,T;L^2(\Gamma_S))$, the weak variational inequality problem of the second kind for (1.1) and (1.2) is proposed as in [2]: Find $\boldsymbol{u}\in L^2(0,T;\boldsymbol{V})\cap L^\infty(0,T,\boldsymbol{Y})$, $p\in L^2(0,T;Q)$ and $\boldsymbol{u}_t(t)\in L^2(0,T;\boldsymbol{Y})$ such that

$$\begin{cases} (\boldsymbol{u}_t,\boldsymbol{v}-\boldsymbol{u}) + a(\boldsymbol{u},\boldsymbol{v}-\boldsymbol{u}) + b(\boldsymbol{u};\boldsymbol{u},\boldsymbol{v}-\boldsymbol{u}) - d(\boldsymbol{v}-\boldsymbol{u},p) + j(\boldsymbol{v}_\tau) - j(\boldsymbol{u}_\tau) \ge (\boldsymbol{f},\boldsymbol{v}-\boldsymbol{u})\ \forall\boldsymbol{v}\in\boldsymbol{V}, \\ d(\boldsymbol{u},q) = 0 \quad \forall q\in Q, \\ \boldsymbol{u}(0) = \boldsymbol{u}_0, \end{cases} \tag{2.1}$$

where $j(\eta) = \int_{\Gamma_S} g(\cdot,t)\,|\eta|\,\mathrm{d}s$, $\eta\in L^2(\Gamma_S)$. Moreover, (2.1) is equivalent to the following problem:

$$\begin{cases} \text{Find} \quad \boldsymbol{u}\in L^2(0,T;\boldsymbol{V}_o)\cap L^\infty(0,T;\boldsymbol{H}) \quad \text{such that} \\ (\boldsymbol{u}_t,\boldsymbol{v}-\boldsymbol{u}) + a(\boldsymbol{u},\boldsymbol{v}-\boldsymbol{u}) + b(\boldsymbol{u};\boldsymbol{u},\boldsymbol{v}-\boldsymbol{u}) + j(\boldsymbol{v}_\tau) - j(\boldsymbol{u}_\tau) \ge (\boldsymbol{f},\boldsymbol{v}-\boldsymbol{u}) \quad \forall\boldsymbol{v}\in\boldsymbol{V}_o, \\ \boldsymbol{u}(0) = \boldsymbol{u}_0. \end{cases} \tag{2.2}$$

Lemma 1 ([14]). *The variational inequality problem (2.2) has a unique solution $\boldsymbol{u}\in L^\infty(0,T;\boldsymbol{V}_o)$, $\boldsymbol{u}_t\in L^\infty(0,T;\boldsymbol{Y})\cap L^2(0,T;\boldsymbol{V}_o)$ if $f\in H^1(0,T;\boldsymbol{Y})$ and $g\in H^1(0,T;L^2(\Gamma_S))$, with $g(0)\in H^1(\Gamma_S)$ and $\boldsymbol{u}_0\in\boldsymbol{H}^2(\Omega)\cap\boldsymbol{V}_o$ which satisfy the slip boundary conditions at $t=0$.*

2.2. The regularized problem and the characteristic method

Define the substantial derivative operator $\mathcal{D}_t\boldsymbol{u} = \frac{\partial\boldsymbol{u}}{\partial t} + (\boldsymbol{u}\cdot\nabla)\boldsymbol{u}$ [19], then the variational inequality problem (2.1) turns into

$$\begin{cases} (\mathcal{D}_t\boldsymbol{u},\boldsymbol{v}-\boldsymbol{u}) + a(\boldsymbol{u},\boldsymbol{v}-\boldsymbol{u}) - d(\boldsymbol{v}-\boldsymbol{u},p) + j(\boldsymbol{v}_\tau) - j(\boldsymbol{u}_\tau) \ge (\boldsymbol{f},\boldsymbol{v}-\boldsymbol{u}) \quad \forall\boldsymbol{v}\in\boldsymbol{V}, \\ d(\boldsymbol{u},q) = 0 \quad \forall q\in Q, \\ \boldsymbol{u}(0) = \boldsymbol{u}_0. \end{cases} \tag{2.3}$$

Now, we introduce a regularized problem of (2.3). Since $j(\eta)$ is not differentiable with respect to η, it is natural to choose a family of functions $j_\varepsilon(\eta)$ which are convex and differentiable to approximate $j(\eta)$ [16]. For any constant $0<\varepsilon\ll 1$, we select

$$j_\varepsilon(\eta) = \int_{\Gamma_S} g\sqrt{|\eta|^2+\varepsilon^2}\,\mathrm{d}s \quad \forall\eta\in L^2(\Gamma_S).$$

Hence $j_\varepsilon(\eta)$ satisfies

$$|j_\varepsilon(\eta) - j(\eta)| \le \varepsilon\int_{\Gamma_S} g\,\mathrm{d}s \quad \forall\eta\in L^2(\Gamma_S)$$

and

$$\langle \mathrm{grad} j_\varepsilon(\eta), \xi\rangle = \lim_{h\to 0}\frac{1}{h}[j_\varepsilon(\eta+h\xi)-j_\varepsilon(\eta)] = \int_{\Gamma_S} g\frac{\eta\xi}{\sqrt{|\eta|^2+\varepsilon^2}}\,\mathrm{d}s \quad \forall \xi,\eta\in L^2(\Gamma_S).$$

Then the regularized problem of (2.3) turns into the following formulation:

$$\begin{cases} \text{Find } \boldsymbol{u}^\varepsilon \in L^2(0,T;\boldsymbol{V})\cap L^\infty(0,T;\boldsymbol{Y}) \text{ and } p^\varepsilon \in L^2(0,T;Q) \text{ such that} \\ (\mathcal{D}_t\boldsymbol{u}^\varepsilon, \boldsymbol{v}-\boldsymbol{u}^\varepsilon) + a(\boldsymbol{u}^\varepsilon, \boldsymbol{v}-\boldsymbol{u}^\varepsilon) - d(\boldsymbol{v}-\boldsymbol{u}^\varepsilon, p^\varepsilon) + j_\varepsilon(\boldsymbol{v}_\tau) - j_\varepsilon(\boldsymbol{u}^\varepsilon_\tau) \geq (\boldsymbol{f}, \boldsymbol{v}-\boldsymbol{u}^\varepsilon) \quad \forall \boldsymbol{v}\in\boldsymbol{V}, \\ d(\boldsymbol{u}^\varepsilon, q) = 0 \quad \forall q\in Q, \\ \boldsymbol{u}^\varepsilon(0) = \boldsymbol{u}_0. \end{cases} \tag{2.4}$$

Since $j_\varepsilon(\eta)$ is convex and differentiable, we use the Gateaux-derivative $K_\varepsilon : \boldsymbol{V}\to\boldsymbol{V}'$ by

$$\langle K_\varepsilon(\boldsymbol{u}), \boldsymbol{v}\rangle = \int_{\Gamma_S} g\frac{\boldsymbol{u}\boldsymbol{v}}{\sqrt{|\boldsymbol{u}|^2+\varepsilon^2}}\,\mathrm{d}s.$$

Hence we can see that K_ε is monotone [13]:

$$\forall\, \boldsymbol{u},\boldsymbol{v}\in\boldsymbol{V} \quad \langle K_\varepsilon(\boldsymbol{u}) - K_\varepsilon(\boldsymbol{v}), \boldsymbol{u}-\boldsymbol{v}\rangle \geq 0.$$

Now the regularized problem (2.4) is equivalent to the following equality problem [13,16]:

$$\begin{cases} (\mathcal{D}_t\boldsymbol{u}^\varepsilon, \boldsymbol{v}) + a(\boldsymbol{u}^\varepsilon, \boldsymbol{v}) - d(\boldsymbol{v}, p^\varepsilon) + \langle K_\varepsilon(\boldsymbol{u}^\varepsilon_\tau), \boldsymbol{v}_\tau\rangle = (\boldsymbol{f}, \boldsymbol{v}) \quad \forall \boldsymbol{v}\in\boldsymbol{V}, \\ d(\boldsymbol{u}^\varepsilon, q) = 0 \quad \forall q\in Q, \\ \boldsymbol{u}^\varepsilon(0) = \boldsymbol{u}_0. \end{cases} \tag{2.5}$$

Moreover, the corresponding characteristic regularized problem of (2.2) can be easily obtained and specifically we do not repeat it here.

3. The characteristic finite element approximation

3.1. Discretization of the material derivative

For a characteristic method, the key lies in the discretization of $\mathcal{D}_t\boldsymbol{u}$. Given the velocity field $\boldsymbol{u}$, we also denote by $X(x, t_{m+1}; t)$ the characteristic curves associated with the material derivative which is defined by the following initial value problem [19]

$$\begin{cases} \dfrac{\mathrm{d}X(x,t_{m+1};t)}{\mathrm{d}t} = \boldsymbol{u}(X(x,t_{m+1};t),t), \\ X(x,t_{m+1};t_{m+1}) = x. \end{cases}$$

Thanks to the Cauchy–Lipschitz Theorem [24], this ODE has a unique solution when $\boldsymbol{u}\in C^{0,1}(\overline{\Omega})^d$, and $X(x,t_{m+1};t)$ represents the position at time t of a particle which locates at x at time t_{m+1}. For all $(x,t)\in\Omega\times[t_m,t_{m+1}]$, $0\leq m\leq M-1$, we have

$$x - X(x,t_{m+1};t_m) = \int_{t_m}^{t_{m+1}} \boldsymbol{u}(X(x,t_{m+1};t),t)\,\mathrm{d}t.$$

If the integral approximation is of first order, then

$$x - X(x,t_{m+1};t_m) \approx \triangle t\,\boldsymbol{u}(X(x,t_{m+1};t_{m+1}),t_{m+1}) = \triangle t\,\boldsymbol{u}(x,t_{m+1}).$$

So, the discretization of the material derivative can be obtained as

$$\mathcal{D}_t\boldsymbol{u}(x,t_{m+1}) \approx \frac{\boldsymbol{u}(x,t_{m+1}) - \boldsymbol{u}(X(x,t_{m+1};t_m),t_m)}{\triangle t}.$$

Here, we leave out some details, one can refer to [19].

3.2. Finite element approximation

Let $\mathcal{T}_h = \{K\}$ be a family of shape-regular and conforming triangulations of Ω and $\overline{\Omega} = \cup_K\overline{K}$ [25], $h = \max\{h_K, h_K = diam(K)\}$ be the grid size. The boundary ∂K of an element consists of faces e. In two dimensions, each e is an edge. The set of all interior edges and $e\in\Gamma_S\cap\partial K$ will be defined by Γ_h with the norm $\|w\|_{\Gamma_h} = \left(\sum_{e\in\Gamma_h}\int_e w^2\mathrm{d}s\right)^{1/2}$ [26]. To construct a Galerkin approximation of (2.5), we consider the following affine FE families

$$\boldsymbol{V}_h := \{\boldsymbol{v}\in\boldsymbol{V}\cap[C^0(\Omega)]^2 : \boldsymbol{v}|_K\in[P_1(K)]^2 \quad \forall K\in\mathcal{T}_h\},$$
$$Q_h = \begin{cases} Q_h^0 := \{q\in Q : q|_K\in P_0(K) \quad \forall K\in\mathcal{T}_h\}, \\ Q_h^1 := \{q\in Q : q|_K\in P_1(K) \quad \forall K\in\mathcal{T}_h\}, \end{cases}$$

where $P_r(K)\,(r = 0, 1)$ denotes the space of polynomials of degree at most r. In the following, we assume that the continuous and discrete spaces are related by the following hypotheses [27]:

(H1). For all $(\boldsymbol{v}, q) \in ([W^{2,\infty}(\Omega)]^2 \cap \boldsymbol{V}, H^1(\Omega) \cap L_0^2(\Omega))$,
$$\inf_{(\boldsymbol{v}_h, q_h)\in \boldsymbol{V}_h\times Q_h} \{\|\nabla(\boldsymbol{v} - \boldsymbol{v}_h)\|_0 + \|q - q_h\|_0\} \le Ch(\|\boldsymbol{v}\|_2 + \|q\|_1),$$
$$\inf_{\boldsymbol{v}_h\in \boldsymbol{V}_h} \|\boldsymbol{v} - \boldsymbol{v}_h\|_{0,\Gamma} \le Ch^2\|\boldsymbol{v}\|_{2,\infty}.$$

We recall a local pressure projection stabilization method to overcome the unstable disadvantage caused by the lower order FE subspaces $\boldsymbol{V}_h \times Q_h$, which establishes an optimal coupling between the velocity and pressure fields such that the weak coerciveness condition is satisfied, as shown in the second lemma [26,28–30]. Let $\Pi_h^j : L^2(\Omega)(j = 0, 1)$ be the standard projection operator [26,28], which is defined as follows:

$$\Pi_h^0 : L^2(\Omega) \to Q_h^0 \quad \text{and} \quad \Pi_h^1 : L^2(\Omega) \to Q_h^1.$$

In case of no distinction, we employ a unified notation Π_h for the valuable projection operator. Then the interpolation error is introduced here and will be used in the theoretical analysis:

$$\|\Pi_h p\|_0 \le \|p\|_0 \ \forall p \in L^2(\Omega) \quad \text{and} \quad \|p - \Pi_h p\|_0 \le Ch\|p\|_1 \quad \forall\, p \in H^1(\Omega) \cap Q.$$

Now, we introduce the stabilization bilinear form $G(p, q)$ in the following manner

$$G(p, q) = (p - \Pi_h p, q - \Pi_h q) \quad \forall p, q \in Q_h.$$

A new FE scheme to approximate (2.5) is given based on the above descriptions.

Definition 1. Suppose that $\boldsymbol{u}_h^{\varepsilon,m}$ and $p_h^{\varepsilon,m}$ are approximations of the velocity and pressure at the point (x, t_m), respectively, and find $(\boldsymbol{u}_h^{\varepsilon,m+1}, p_h^{\varepsilon,m+1}) \in \boldsymbol{V}_h \times Q_h$ such that

$$\begin{aligned}(\mathrm{d}_t \boldsymbol{u}_h^{\varepsilon,m+1}, \boldsymbol{v}_h) + a(\boldsymbol{u}_h^{\varepsilon,m+1}, \boldsymbol{v}_h) - d(\boldsymbol{v}_h, p_h^{\varepsilon,m+1}) + \langle K_\varepsilon(\boldsymbol{u}_{h\boldsymbol{\tau}}^{\varepsilon,m+1}), \boldsymbol{v}_{h\boldsymbol{\tau}}\rangle &= (\boldsymbol{f}^{m+1}, \boldsymbol{v}_h) \quad \forall \boldsymbol{v}_h \in \boldsymbol{V}_h,\\ d(\boldsymbol{u}_h^{\varepsilon,m+1}, q_h) + G(p_h^{\varepsilon,m+1}, q_h) &= 0 \quad \forall q_h \in Q_h,\end{aligned} \tag{3.1}$$

where

$$\mathrm{d}_t \boldsymbol{u}_h^{\varepsilon,m+1}(x) = \frac{\boldsymbol{u}_h^{\varepsilon,m+1}(x) - \boldsymbol{u}_h^{\varepsilon,m}(X_h^m(x, t_{m+1}; t_m))}{\triangle t}$$

and $X_h^m(x, t_{m+1}; t_m)$ is the solution of

$$\begin{cases}\dfrac{\mathrm{d}X_h^m(x, t_{m+1}; t)}{\mathrm{d}t} = \boldsymbol{u}_h^{\varepsilon,m}(X_h^m(x, t_{m+1}; t), t) \quad t_m \le t \le t_{m+1},\\ X_h^m(x, t_{m+1}; t_{m+1}) = x.\end{cases}$$

The initial approximate velocity $\boldsymbol{u}_{0h}^\varepsilon$ will be chosen to be the $\boldsymbol{V}$-projection of $\boldsymbol{u}_0^\varepsilon$ onto $\boldsymbol{V}_h$. If $\boldsymbol{u}_0^\varepsilon \in H^2(\Omega) \cap \boldsymbol{V}$, there exists a positive constant C such that

$$\|\boldsymbol{u}_0^\varepsilon - \boldsymbol{u}_{0h}^\varepsilon\|_0 + h\|\nabla(\boldsymbol{u}_0^\varepsilon - \boldsymbol{u}_{0h}^\varepsilon)\|_0 \le Ch^2. \tag{3.2}$$

Remark 1. (a). If the FE subspace $\boldsymbol{V}_h \times Q_h^0$ is chosen, the stabilized term $G(p_h, q_h) = (p_h - \Pi_h^1 p_h, q_h - \Pi_h^1 q_h)$, and when we select $\boldsymbol{V}_h \times Q_h^1$, $G(p_h, q_h) = (p_h - \Pi_h^0 p_h, q_h - \Pi_h^0 q_h)$. The detailed implementation of Π_h^j, $(j = 0, 1)$ can be found in [12,26].

(b). The characteristic stabilized FE approximation of problem (2.3) can be displayed as similarly: Find $(\boldsymbol{u}_h, p_h) \in \boldsymbol{V}_h \times Q_h$, for all $(\boldsymbol{v}_h, q_h) \in \boldsymbol{V}_h \times Q_h$, such that

$$\begin{cases}(\mathrm{d}_t \boldsymbol{u}_h, \boldsymbol{v}_h - \boldsymbol{u}_h,) + a(\boldsymbol{u}_h, \boldsymbol{v}_h - \boldsymbol{u}_h,) - d(\boldsymbol{v}_h - \boldsymbol{u}_h, p_h) + j_h(\boldsymbol{v}_{h\boldsymbol{\tau}}) - j_h(\boldsymbol{u}_{h\boldsymbol{\tau}}) \ge (\boldsymbol{f}, \boldsymbol{v}_h - \boldsymbol{u}_h),\\ d(\boldsymbol{u}_h, q_h) + G(p_h, q_h) = 0.\end{cases} \tag{3.3}$$

We denote $\mathcal{B}_h((\boldsymbol{u}_h, p_h); (\boldsymbol{v}_h, q_h)) = a(\boldsymbol{u}_h, \boldsymbol{v}_h) - d(\boldsymbol{v}_h, p_h) + d(\boldsymbol{u}_h, q_h) + G(p_h, q_h)$, $(\boldsymbol{u}_h, p_h), (\boldsymbol{v}_h, q_h) \in \boldsymbol{V}_h \times Q_h$, and recall the following stability lemma:

Lemma 2 (*[28,30]*). *There exist positive constants β_1, β_2, independent of h, $\forall(\boldsymbol{u}_h, p_h) \in \boldsymbol{V}_h \times Q_h$ such that,*

$$|\mathcal{B}_h((\boldsymbol{u}_h, p_h); (\boldsymbol{v}_h, q_h))| \le \beta_1(\|\nabla \boldsymbol{u}_h\|_0 + \|p_h\|_0)(\|\nabla \boldsymbol{v}_h\|_0 + \|q_h\|_0) \ \forall(\boldsymbol{v}_h, q_h) \in \boldsymbol{V}_h \times Q_h,$$
$$\beta_2(\|\nabla \boldsymbol{u}_h\|_0 + \|p_h\|_0) \le \sup_{0\ne(\boldsymbol{v}_h, q_h)\in \overset{\circ}{\boldsymbol{V}}_h\times Q_h} \frac{\mathcal{B}_h((\boldsymbol{u}_h, p_h); (\boldsymbol{v}_h, q_h))}{\|\nabla \boldsymbol{v}_h\|_0 + \|q_h\|_0},$$

where $\overset{\circ}{\boldsymbol{V}}_h = \{\boldsymbol{v} \in \overset{\circ}{\boldsymbol{V}} : \boldsymbol{v}|_K \in \boldsymbol{P}_1(K)\ \forall K \in \mathcal{T}_h\}$ is a FE subspace of $\overset{\circ}{\boldsymbol{V}}$.

The system of equations (3.1) is symmetric and this characteristic FE scheme is unconditionally stable provided that the characteristics are transported by a divergence-free field. Indeed, as in [31], choosing $(\boldsymbol{v}_h, q_h) = (\boldsymbol{u}_h^{\varepsilon,m+1}, p_h^{\varepsilon,m+1})$ in (3.1) gives

$$\begin{aligned}&\|\boldsymbol{u}_h^{\varepsilon,m+1}\|_0^2 + \nu\triangle t\|\nabla\boldsymbol{u}_h^{\varepsilon,m+1}\|_0^2 + \triangle t\|(I-\Pi_h)p_h^{\varepsilon,m+1}\|_0^2 + \triangle t\langle K_\varepsilon(\boldsymbol{u}_{h\tau}^{\varepsilon,m+1}), \boldsymbol{u}_h^{\varepsilon,m+1}\rangle\\ &= \triangle t(\boldsymbol{f}^{m+1}, \boldsymbol{u}_h^{\varepsilon,m+1}) + (\boldsymbol{u}_h^{\varepsilon,m}(X_h^m(x,t_{m_1};t_m)), \boldsymbol{u}_h^{\varepsilon,m+1}).\end{aligned}$$

Using Young's inequality and the definition of K_ε, one obtains

$$\begin{aligned}&\|\boldsymbol{u}_h^{\varepsilon,m+1}\|_0^2 + \nu\triangle t\|\nabla\boldsymbol{u}_h^{\varepsilon,m+1}\|_0^2 + \triangle t\|(I-\Pi_h)p_h^{\varepsilon,m+1}\|_0^2 + \triangle t\int_{\Gamma_S} g\frac{(\boldsymbol{u}_{h\tau}^{\varepsilon,m+1})^2}{\sqrt{|\boldsymbol{u}_{h\tau}^{\varepsilon,m+1}|^2+\varepsilon^2}}\,\mathrm{d}s\\ &\le C(\triangle t\|\boldsymbol{f}^{m+1}\|_0^2 + \|\boldsymbol{u}_h^{\varepsilon,m}\|_0^2).\end{aligned}$$

Furthermore, we see that

$$\begin{aligned}&\left\{\|\boldsymbol{u}_h^{\varepsilon,m+1}\|_0^2 + \nu\triangle t\|\nabla\boldsymbol{u}_h^{\varepsilon,m+1}\|_0^2 + \triangle t\|(I-\Pi_h)p_h^{\varepsilon,m+1}\|_0^2 + \triangle t\int_{\Gamma_S} g\frac{(\boldsymbol{u}_{h\tau}^{\varepsilon,m+1})^2}{\sqrt{|\boldsymbol{u}_{h\tau}^{\varepsilon,m+1}|^2+\varepsilon^2}}\,\mathrm{d}s\right\}^{\frac{1}{2}}\\ &\le C(\triangle t\|\boldsymbol{f}^{m+1}\|_0 + \|\boldsymbol{u}_h^{\varepsilon,m}\|_0).\end{aligned}$$

Namely,

$$\begin{aligned}&\left\{\|\boldsymbol{u}_h^{\varepsilon,m+1}\|_0^2 + \nu\triangle t\|\nabla\boldsymbol{u}_h^{\varepsilon,m+1}\|_0^2 + \triangle t\int_{\Gamma_S} g\frac{(\boldsymbol{u}_{h\tau}^{\varepsilon,m+1})^2}{\sqrt{|\boldsymbol{u}_{h\tau}^{\varepsilon,m+1}|^2+\varepsilon^2}}\,\mathrm{d}s\right\}^{\frac{1}{2}}\\ &\le C\triangle t\|\boldsymbol{f}^{m+1}\|_0 + C\left\{\|\boldsymbol{u}_h^{\varepsilon,m}\|_0^2 + \nu\triangle t\|\nabla\boldsymbol{u}_h^{\varepsilon,m}\|_0^2 + \triangle t\int_{\Gamma_S} g\frac{(\boldsymbol{u}_{h\tau}^{\varepsilon,m})^2}{\sqrt{|\boldsymbol{u}_{h\tau}^{\varepsilon,m}|^2+\varepsilon^2}}\,\mathrm{d}s\right\}^{\frac{1}{2}},\end{aligned}$$

so the stability of this discrete scheme is proved.

3.3. Existence and uniqueness of a solution to the regularized discrete scheme

Lemma 3. *There exists a unique solution pair $(\boldsymbol{u}_h^\varepsilon, p_h^\varepsilon) \in \boldsymbol{V}_h \times Q_h$ to problem (3.1).*

Proof. Assume that $\boldsymbol{V}_h$ and Q_h are the spaces defined as above. We introduce the following formulas [26]:

$$\sup_{0\neq\boldsymbol{v}_h\in\boldsymbol{V}_h}\frac{\int_\Omega p_h\,\mathrm{div}\,\boldsymbol{v}_h\,\mathrm{d}\boldsymbol{x}}{\|\nabla\boldsymbol{v}_h\|_0} \ge C_1\|p_h\|_0 - C_2\|p_h - \Pi_h p_h\|_0 \quad \forall p_h \in Q_h.$$

Considering that existence is equivalent to uniqueness of a solution for a finite-dimensional linear system, using induction and following [32], one can complete the proof.

4. Error estimates

The objective of this section is to derive optimal error estimates for the characteristic stabilized method. To begin with, we suppose that

$$\boldsymbol{f} \in C(0,T;H), \quad \boldsymbol{u}_0^\varepsilon \in \boldsymbol{H}(0,T;\boldsymbol{V}) \cap C\Big(0,T;\boldsymbol{C}^{0,1}(\overline{\Omega})\Big).$$

The corresponding solution $(\boldsymbol{u}^\varepsilon, p^\varepsilon)$ of problem (2.5) will be assumed to satisfy the following regularity hypotheses [19,33]:

(H2). $\boldsymbol{u}^\varepsilon \in L^\infty\Big(0,T,\boldsymbol{H}^2(\Omega)\Big) \cap C\Big(0,T;\boldsymbol{C}^{0,1}(\overline{\Omega})\Big) \cap C(0,T;\boldsymbol{V})$,

(H3). $\dfrac{\mathrm{d}\boldsymbol{u}^\varepsilon}{\mathrm{d}t} \in L^2\Big(0,T;\boldsymbol{H}^2(\Omega)\Big) \cap L^2(0,T;\boldsymbol{H}) \cap L^2(0,T;\boldsymbol{V}_o), \quad \mathcal{D}_t^2\boldsymbol{u}^\varepsilon \in L^2(0,T;\boldsymbol{H})$,

(H4). $p^\varepsilon \in L^\infty\Big(0,T;H^1(\Omega)\Big) \cap L^\infty(0,T;Q), \quad \dfrac{\mathrm{d}p^\varepsilon}{\mathrm{d}t} \in L^2(0,T;H^1(\Omega))$,

(H5). Let us make the mesh restriction $\triangle t = \mathcal{O}(h^\varrho)$, as $h \to 0$, where $\varrho > 1/2$. Moreover, for the sufficiently small ε, holds $\varepsilon^2 < C(\boldsymbol{u}_\tau^\varepsilon)^3$ on Γ_S.

Now we introduce the Galerkin projection operator $(\mathcal{R}_h, \mathcal{Q}_h) : (\boldsymbol{V}, Q) \longrightarrow (\boldsymbol{V}_h, Q_h)$ as

$$\mathcal{B}_h((\mathcal{R}_h(\boldsymbol{u},p), \mathcal{Q}_h(\boldsymbol{u},p)); (\boldsymbol{v}_h, q_h)) = \mathcal{B}((\boldsymbol{u},p);(\boldsymbol{v}_h,q_h)) \quad \forall(\boldsymbol{v}_h,q_h) \in \boldsymbol{V}_h \times Q_h,$$

where $\mathcal{B}((\boldsymbol{u}, p); (\boldsymbol{v}, q)) = a(\boldsymbol{u}, \boldsymbol{v}) - d(\boldsymbol{v}, p) + d(\boldsymbol{u}, q)$. It is well defined and satisfies (H1)[27,28]. At this point, the initial value can be chosen as $\boldsymbol{u}_{0h}^{\varepsilon} = \mathcal{R}_h(\boldsymbol{u}_0, p_0)$ and $p_{0h}^{\varepsilon} = \mathcal{Q}(\boldsymbol{u}_0, p_0)$.

We will frequently use a discrete version of the Gronwall's lemma used in [33].

Lemma 4. *Let C, $\triangle t$, and a_n, b_n, c_n, d_n, for integers $n \geq 0$, be nonnegative numbers such that*

$$a_m + \triangle t \sum_{n=0}^{m} b_n \leq \triangle t \sum_{n=0}^{m} a_n d_n + \triangle t \sum_{n=0}^{m} c_n + C \quad \forall m \geq 1.$$

Suppose that $\triangle t d_n < 1$, for all n, and set $\gamma_n \equiv (1 - \triangle t d_n)^{-1}$. Then

$$a_m + \triangle t \sum_{n=0}^{m} b_n \leq exp\left(\triangle t \sum_{n=0}^{m} \gamma_n d_n\right)\left(\triangle t \sum_{n=0}^{m} c_n + C\right) \quad \forall m \geq 1.$$

4.1. L^2 and H^1 estimates for velocity

Theorem 5. *Under assumptions (H1)-(H5), there exists a positive constant C, independent of h and $\triangle t$, such that*

$$\|\boldsymbol{u}^{\varepsilon} - \boldsymbol{u}_h^{\varepsilon}\|_{l^{\infty}(0,T;\boldsymbol{L}^2(\Omega))} \leq C(\triangle t + h^2).$$

Proof. According to (3.2), we see that

$$\|\boldsymbol{u}^{\varepsilon}(\cdot, t_0) - \boldsymbol{u}_{0h}^{\varepsilon}\|_0 \leq C(\triangle t + h^2), \quad \|\nabla(\boldsymbol{u}^{\varepsilon}(\cdot, t_0) - \boldsymbol{u}_{0h}^{\varepsilon})\|_0 \leq C(\triangle t + h). \tag{4.1}$$

Introduce the functions $\boldsymbol{\phi}^{\varepsilon} = \boldsymbol{u}^{\varepsilon} - \boldsymbol{u}_h^{\varepsilon}$, $\boldsymbol{\delta}^{\varepsilon} = \boldsymbol{u}^{\varepsilon} - \mathcal{R}_h$, $\boldsymbol{\sigma}^{\varepsilon} = \boldsymbol{\delta}^{\varepsilon} - \boldsymbol{\phi}^{\varepsilon}$, $\zeta^{\varepsilon} = p_h^{\varepsilon} - \mathcal{Q}_h$, where $\mathcal{R}_h \triangleq \mathcal{R}_h(\boldsymbol{u}^{\varepsilon}, p^{\varepsilon})$, $\mathcal{Q}_h \triangleq \mathcal{Q}_h(\boldsymbol{u}^{\varepsilon}, p^{\varepsilon})$. Subtracting (3.1) from (2.5) with $(\boldsymbol{v}, q) = (\boldsymbol{v}_h, q_h)$ yields

$$\begin{aligned}
&(\mathrm{d}_t\boldsymbol{\sigma}^{\varepsilon,m+1}, \boldsymbol{v}_h) + a(\boldsymbol{\sigma}^{\varepsilon,m+1}, \boldsymbol{v}_h) - d(\boldsymbol{v}_h, \zeta^{\varepsilon,m+1}) + d(\boldsymbol{\sigma}^{\varepsilon,m+1}, q_h) + G(\zeta^{\varepsilon,m+1}, q_h)\\
&\quad = \langle K_{\varepsilon}(\boldsymbol{u}_{\boldsymbol{\tau}}^{\varepsilon}(\cdot, t_{m+1})) - K_{\varepsilon}(\boldsymbol{u}_{h\boldsymbol{\tau}}^{\varepsilon,m+1}), \boldsymbol{v}_h\rangle + (\mathrm{d}_t\boldsymbol{\delta}^{\varepsilon}(\cdot, t_{m+1}), \boldsymbol{v}_h) + (\mathcal{D}_t\boldsymbol{u}^{\varepsilon}(\cdot, t_{m+1}) - \mathrm{d}_t\boldsymbol{u}^{\varepsilon}(\cdot, t_{m+1}), \boldsymbol{v}_h).
\end{aligned} \tag{4.2}$$

Choosing $(\boldsymbol{v}_h, q_h) = (\boldsymbol{\sigma}^{\varepsilon,m+1}, \zeta^{\varepsilon,m+1})$ in (4.2) gives

$$\begin{aligned}
&(\mathrm{d}_t\boldsymbol{\sigma}^{\varepsilon,m+1}, \boldsymbol{\sigma}^{\varepsilon,m+1}) + \nu\|\nabla\boldsymbol{\sigma}^{\varepsilon,m+1}\|_0^2 + \|(I - \Pi_h)\zeta^{\varepsilon,m+1}\|_0^2\\
&= \langle K_{\varepsilon}(\boldsymbol{u}_{\boldsymbol{\tau}}^{\varepsilon}(\cdot, t_{m+1})) - K_{\varepsilon}(\boldsymbol{u}_{h\boldsymbol{\tau}}^{\varepsilon,m+1}), \boldsymbol{\sigma}^{\varepsilon,m+1}\rangle + (\mathrm{d}_t\boldsymbol{\delta}^{\varepsilon}(\cdot, t_{\varepsilon,m+1}), \boldsymbol{\sigma}^{\varepsilon,m+1})\\
&\quad + (\mathcal{D}_t\boldsymbol{u}^{\varepsilon}(\cdot, t_{m+1}) - \mathrm{d}_t\boldsymbol{u}^{\varepsilon}(\cdot, t_{m+1}), \boldsymbol{\sigma}^{\varepsilon,m+1}).
\end{aligned} \tag{4.3}$$

Hence, using $2(x - y, x) \geq |x|^2 - |y|^2$, (4.3) turns into

$$\begin{aligned}
&\frac{1}{2\triangle t}(\|\boldsymbol{\sigma}^{\varepsilon,m+1}\|_0^2 - \|\boldsymbol{\sigma}^{\varepsilon,m}\|_0^2) + \nu\|\nabla\boldsymbol{\sigma}^{\varepsilon,m+1}\|_0^2 + \|(I - \Pi_h)\zeta^{\varepsilon,m+1}\|_0^2\\
&\leq \left|\left(\mathcal{D}_t\boldsymbol{u}^{\varepsilon}(\cdot, t_{m+1}) - \frac{\boldsymbol{u}^{\varepsilon}(\cdot, t_{m+1}) - \boldsymbol{u}^{\varepsilon}(X(\cdot, t_{m+1}; t_m), t_m)}{\triangle t}, \boldsymbol{\sigma}^{\varepsilon,m+1}\right)\right| + \left|\left(\frac{\boldsymbol{\delta}^{\varepsilon}(\cdot, t_{m+1}) - \boldsymbol{\delta}^{\varepsilon}(\cdot, t_m)}{\triangle t}, \boldsymbol{\sigma}^{\varepsilon,m+1}\right)\right|\\
&\quad + \left|\left(\frac{\boldsymbol{u}^{\varepsilon}(X(\cdot, t_{m+1}; t_m), t_m) - \boldsymbol{u}^{\varepsilon}(X_h^m(\cdot, t_{m+1}; t_m), t_m)}{\triangle t}, \boldsymbol{\sigma}^{\varepsilon,m+1}\right)\right|\\
&\quad + \left|\left(\frac{\boldsymbol{\delta}^{\varepsilon}(\cdot, t_m) - \boldsymbol{\delta}^{\varepsilon}(X(\cdot, t_{m+1}; t_m), t_m)}{\triangle t}, \boldsymbol{\sigma}^{\varepsilon,m+1}\right)\right|\\
&\quad + \left|\left(\frac{\boldsymbol{\delta}^{\varepsilon}(X(\cdot, t_{m+1}; t_m), t_m) - \boldsymbol{\delta}^{\varepsilon}(X_h^m(\cdot, t_{m+1}; t_m), t_m)}{\triangle t}, \boldsymbol{\sigma}^{\varepsilon,m+1}\right)\right|\\
&\quad + \left|\left(\frac{\boldsymbol{\sigma}^{\varepsilon,m}(\cdot) - \boldsymbol{\sigma}^{\varepsilon,m}(X(\cdot, t_{m+1}; t_m))}{\triangle t}, \boldsymbol{\sigma}^{\varepsilon,m+1}\right)\right| + \left|\left(\frac{\boldsymbol{\sigma}^{\varepsilon,m}(X(\cdot, t_{m+1}; t_m)) - \boldsymbol{\sigma}^{\varepsilon,m}(X_h^m(\cdot, t_{m+1}; t_m))}{\triangle t}, \boldsymbol{\sigma}^{\varepsilon,m+1}\right)\right|\\
&\quad + |\langle K_{\varepsilon}(\boldsymbol{u}_{\boldsymbol{\tau}}^{\varepsilon}(\cdot, t_{m+1})) - K_{\varepsilon}(\boldsymbol{u}_{h\boldsymbol{\tau}}^{\varepsilon,m+1}), \boldsymbol{\sigma}^{\varepsilon,m+1}\rangle| = \sum_{i=1}^{8} I_i.
\end{aligned} \tag{4.4}$$

Following [19] and using a scaling argument, we obtain the estimates for I_i $(i = 1, \ldots, 7)$ and summing them up, there holds

$$\begin{aligned}
\sum_{i=1}^{7} I_i \leq\ & \epsilon_1\|\boldsymbol{\sigma}^{\varepsilon,m+1}\|_0^2 + \frac{4\epsilon_2}{5}\|\nabla\boldsymbol{\sigma}^{\varepsilon,m+1}\|_0^2 + C\triangle t\|\mathcal{D}_t^2\boldsymbol{u}^{\varepsilon}\|_{L^2(t_m,t_{m+1};\boldsymbol{Y})}^2 + C\triangle t\left\|\frac{\mathrm{d}\boldsymbol{u}^{\varepsilon}}{\mathrm{d}t}\right\|_{L^2(t_m,t_{m+1};\boldsymbol{Y})}^2\\
&+ C\|\boldsymbol{\phi}^{\varepsilon,m}\|_0^2 + \frac{C}{\triangle t}\left\|\frac{\mathrm{d}\boldsymbol{\delta}^{\varepsilon}}{\mathrm{d}t}\right\|_{L^2(t_m,t_{m+1};\boldsymbol{Y})}^2 + C\|\boldsymbol{\delta}^{\varepsilon}\|_{L^{\infty}(\boldsymbol{Y})} + C\|\boldsymbol{\sigma}^{\varepsilon,m}\|_0^2.
\end{aligned}$$

Next, we estimate I_8 in terms of the mean-value theorem:

$$\begin{aligned}
&\langle K_\varepsilon(\boldsymbol{u}_{\boldsymbol{\tau}}^{\varepsilon}(\cdot,t_{m+1}))-K_\varepsilon(\boldsymbol{u}_{h\boldsymbol{\tau}}^{\varepsilon,m+1}),\boldsymbol{\sigma}^{\varepsilon,m+1}\rangle=\langle K_\varepsilon(\boldsymbol{u}_{\boldsymbol{\tau}}^{\varepsilon}(\cdot,t_{m+1}))-K_\varepsilon(\boldsymbol{u}_{h\boldsymbol{\tau}}^{\varepsilon,m+1}),\boldsymbol{u}_{h\boldsymbol{\tau}}^{\varepsilon,m+1}-\boldsymbol{u}_{\boldsymbol{\tau}}^{\varepsilon}(\cdot,t_{m+1})\rangle\\
&\quad+\langle K_\varepsilon(\boldsymbol{u}_{\boldsymbol{\tau}}^{\varepsilon}(\cdot,t_{m+1}))-K_\varepsilon(\boldsymbol{u}_{h\boldsymbol{\tau}}^{\varepsilon,m+1}),\boldsymbol{u}_{\boldsymbol{\tau}}^{\varepsilon}(\cdot,t_{m+1})-\mathcal{R}_{h\boldsymbol{\tau}}^{m+1}\rangle\\
&\le\langle K_\varepsilon(\boldsymbol{u}_{\boldsymbol{\tau}}^{\varepsilon}(\cdot,t_{m+1}))-K_\varepsilon(\boldsymbol{u}_{h\boldsymbol{\tau}}^{\varepsilon,m+1}),\boldsymbol{u}_{\boldsymbol{\tau}}^{\varepsilon}(\cdot,t_{m+1})-\mathcal{R}_{h\boldsymbol{\tau}}^{m+1}\rangle\\
&=\int_{\Gamma_S}g\left(\frac{\boldsymbol{u}_{\boldsymbol{\tau}}^{\varepsilon}(\cdot,t_{m+1})}{\sqrt{|\boldsymbol{u}_{\boldsymbol{\tau}}^{\varepsilon}(\cdot,t_{m+1})|^2+\varepsilon^2}}-\frac{\boldsymbol{u}_{h\boldsymbol{\tau}}^{\varepsilon,m+1}}{\sqrt{|\boldsymbol{u}_{h\boldsymbol{\tau}}^{\varepsilon,m+1}|^2+\varepsilon^2}}\right)\cdot(\boldsymbol{u}_{\boldsymbol{\tau}}^{\varepsilon}(\cdot,t_{m+1})-\mathcal{R}_{h\boldsymbol{\tau}}^{m+1})\,\mathrm{d}s\\
&\le\int_{\Gamma_S}|g|\frac{\varepsilon^2}{(|\widetilde{\boldsymbol{u}_{h\boldsymbol{\tau}}^{\varepsilon}}(\cdot,t_{m+1})|^2+\varepsilon^2)^{3/2}}\cdot|\boldsymbol{u}_{\boldsymbol{\tau}}^{\varepsilon}(\cdot,t_{m+1})-\boldsymbol{u}_{h\boldsymbol{\tau}}^{\varepsilon,m+1}|\cdot|\boldsymbol{u}_{\boldsymbol{\tau}}^{\varepsilon}(\cdot,t_{m+1})-\mathcal{R}_{h\boldsymbol{\tau}}^{m+1}|\mathrm{d}s,
\end{aligned}$$

where $\widetilde{\boldsymbol{u}_{h\boldsymbol{\tau}}^{\varepsilon}}$ lies between $\boldsymbol{u}_{h\boldsymbol{\tau}}^{\varepsilon}$ and $\boldsymbol{u}_{\boldsymbol{\tau}}^{\varepsilon}$. Using hypothesis (H1), for sufficiently small $\varepsilon>0$, holds

$$\begin{aligned}
I_8&=|\langle K_\varepsilon(\boldsymbol{u}_{\boldsymbol{\tau}}^{\varepsilon}(\cdot,t_{m+1}))-K_\varepsilon(\boldsymbol{u}_{h\boldsymbol{\tau}}^{\varepsilon,m+1}),\boldsymbol{\sigma}^{\varepsilon,m+1}\rangle|\\
&\le C\|g\|_{L^\infty(\Gamma_S)}(\|\boldsymbol{u}_{h\boldsymbol{\tau}}^{\varepsilon,m+1}-\mathcal{R}_{h\boldsymbol{\tau}}^{m+1}\|_{0,\Gamma_S}+\|\boldsymbol{u}_{\boldsymbol{\tau}}^{\varepsilon}(\cdot,t_{m+1})-\mathcal{R}_{h\boldsymbol{\tau}}^{m+1}\|_{0,\Gamma_S})\|\boldsymbol{u}_{\boldsymbol{\tau}}^{\varepsilon}(\cdot,t_{m+1})-\mathcal{R}_{h\boldsymbol{\tau}}^{m+1}\|_{0,\Gamma_S}\\
&\le Ch^4\|\boldsymbol{u}^{\varepsilon}\|_{2,\infty}+Ch^2\|\nabla\boldsymbol{\sigma}^{\varepsilon,m+1}\|_0\|\boldsymbol{u}^{\varepsilon}\|_{2,\infty}\le Ch^4+\frac{\epsilon_2}{5}\|\nabla\boldsymbol{\sigma}^{\varepsilon,m+1}\|_0^2.
\end{aligned}$$

Substituting the above estimates into Eq. (4.4), multiplying the resulting inequality by $2\triangle t$, summing 0 to n for index m, and choosing $\epsilon_1=\frac{1}{4T}$ and $\epsilon_2=\frac{\nu}{2}$, we obtain the recursive relation:

$$\begin{aligned}
&\|\boldsymbol{\sigma}^{\varepsilon,n+1}\|_0^2+\nu\triangle t\sum_{m=0}^{n+1}\|\nabla\boldsymbol{\sigma}^{\varepsilon,m}\|_0^2+2\triangle t\sum_{m=0}^{n}\|(I-\Pi_h)\zeta^{\varepsilon,m+1}\|_0^2\\
&\le C\triangle t^2\left(\|\mathcal{D}_t^2\boldsymbol{u}^{\varepsilon}\|_{L^2(0,T;\boldsymbol{Y})}^2+\left\|\frac{\mathrm{d}\boldsymbol{u}^{\varepsilon}}{\mathrm{d}t}\right\|_{L^2(0,T;\boldsymbol{Y})}^2\right)+C\left(\|\boldsymbol{\delta}^{\varepsilon}\|_{L^\infty(0,T;\boldsymbol{Y})}^2+\left\|\frac{\mathrm{d}\boldsymbol{\delta}^{\varepsilon}}{\mathrm{d}t}\right\|_{L^2(0,T;\boldsymbol{Y})}^2\right)\\
&\quad+C\triangle t\sum_{m=0}^{n}\|\boldsymbol{\phi}^{\varepsilon,m}\|_0^2+C\triangle t\sum_{m=0}^{n}\|\boldsymbol{\sigma}^{\varepsilon,m}\|_0^2+Ch^4.
\end{aligned}$$

By assumption (H1), using the discrete Gronwall's lemma, and the triangle inequality, we see that

$$\begin{aligned}
\|\boldsymbol{\phi}^{\varepsilon,n+1}\|_0^2\le\ &2\|\boldsymbol{\sigma}^{\varepsilon,n+1}\|_0^2+2\|\boldsymbol{\delta}^{\varepsilon,n+1}\|_0^2\le C\triangle t^2\left(\|\mathcal{D}_t^2\boldsymbol{u}^{\varepsilon}\|_{L^2(0,T;\boldsymbol{Y})}^2+\left\|\frac{\mathrm{d}\boldsymbol{u}^{\varepsilon}}{\mathrm{d}t}\right\|_{L^2(0,T;\boldsymbol{Y})}^2\right)\\
&+Ch^4\left(\|\boldsymbol{u}^{\varepsilon}\|_{L^\infty(0,T;\boldsymbol{Y})}^2+\left\|\frac{\mathrm{d}\boldsymbol{u}^{\varepsilon}}{\mathrm{d}t}\right\|_{L^2(0,T;\boldsymbol{Y})}^2+\|p^{\varepsilon}\|_{L^\infty(0,T;H^1(\Omega))}^2+\left\|\frac{\mathrm{d}p^{\varepsilon}}{dt}\right\|_{L^2(0,T;H^1(\Omega))}^2\right)\\
&+C\triangle t\sum_{m=0}^{n}\|\boldsymbol{\phi}^{\varepsilon,m}\|_0^2.
\end{aligned}$$

Finally, the discrete version of Lemma 4 completes this proof.

Theorem 6. *When* (H1)–(H5) *hold and further assume that the grid size h and time size $\triangle t$ satisfy*

$$\text{(a) } h^2\le C_7-2C_6\quad\textit{and}\quad\text{(b) }\triangle t\le\frac{C_7-2C_6}{C_7}\quad(2C_6<C_7),$$

where C_6, C_7 are positive constants independent of h and $\triangle t$, then we have the following estimate

$$\|\boldsymbol{u}^{\varepsilon}-\boldsymbol{u}_h^{\varepsilon}\|_{l^\infty(0,T;\boldsymbol{V})}\le C(\triangle t+h).$$

Remark 2. The reason of the existences of (a) and (b) is that we need to control the estimates for divergence term $d(\cdot,\cdot)$ by the stabilized term and $\|\frac{\boldsymbol{\sigma}^{\varepsilon,m}}{\triangle t}\|_0^2$ in the following proof, which is a special treatment in this theorem. And if putting (a) (b) together, one can see that delta $t=O(h^2)$, which is not conflicting to (H5).

Proof. Taking $\boldsymbol{v}_h=\frac{\boldsymbol{\sigma}^{\varepsilon,m+1}-\boldsymbol{\sigma}^{\varepsilon,m}}{\triangle t}$ and $q_h=\frac{\zeta^{\varepsilon,m+1}}{\triangle t}$ in Eq. (4.2), we have

$$\begin{aligned}
&\left\|\frac{\boldsymbol{\sigma}^{\varepsilon,m+1}-\boldsymbol{\sigma}^{\varepsilon,m}}{\triangle t}\right\|_0^2+\frac{\nu}{2\triangle t}(\|\nabla\boldsymbol{\sigma}^{\varepsilon,m+1}\|_0^2-\|\nabla\boldsymbol{\sigma}^{\varepsilon,m}\|_0^2)+d\left(\frac{\boldsymbol{\sigma}^{\varepsilon,m}}{\triangle t},\zeta^{\varepsilon,m+1}\right)+\frac{1}{\triangle t}\|(I-\Pi_h)\zeta^{\varepsilon,m+1}\|_0^2\\
&+\frac{\nu}{2}\left\|\nabla\left(\frac{\boldsymbol{\sigma}^{\varepsilon,m+1}-\boldsymbol{\sigma}^{\varepsilon,m}}{\triangle t^{\frac{1}{2}}}\right)\right\|_0^2\le\left|\left(\mathcal{D}_t\boldsymbol{u}^{\varepsilon}(\cdot,t_{m+1})-\frac{\boldsymbol{u}^{\varepsilon}(\cdot,t_{m+1})-\boldsymbol{u}^{\varepsilon}(X(\cdot,t_{m+1};t_m),t_m)}{\triangle t},\frac{\boldsymbol{\sigma}^{\varepsilon,m+1}-\boldsymbol{\sigma}^{\varepsilon,m}}{\triangle t}\right)\right|\\
&+\left|\left(\frac{\boldsymbol{u}^{\varepsilon}(X(\cdot,t_{m+1};t_m),t_m)-\boldsymbol{u}^{\varepsilon}(X_h^m(\cdot,t_{m+1};t_m),t_m)}{\triangle t},\frac{\boldsymbol{\sigma}^{\varepsilon,m+1}-\boldsymbol{\sigma}^{\varepsilon,m}}{\triangle t}\right)\right|
\end{aligned}$$

$$
\begin{aligned}
&+\left|\Big(\frac{\boldsymbol{\delta}^{\varepsilon}(\cdot,t_{m+1})-\boldsymbol{\delta}^{\varepsilon}(\cdot,t_m)}{\triangle t},\frac{\boldsymbol{\sigma}^{\varepsilon,m+1}-\boldsymbol{\sigma}^{\varepsilon,m}}{\triangle t}\Big)\right|+\left|\Big(\frac{\boldsymbol{\delta}^{\varepsilon}(\cdot,t_m)-\boldsymbol{\delta}^{\varepsilon}(X(\cdot,t_{m+1};t_m),t_m)}{\triangle t},\frac{\boldsymbol{\sigma}^{\varepsilon,m+1}-\boldsymbol{\sigma}^{\varepsilon,m}}{\triangle t}\Big)\right|\\
&+\left|\Big(\frac{\boldsymbol{\delta}^{\varepsilon}(X(\cdot,t_{m+1};t_m),t_m)-\boldsymbol{\delta}^{\varepsilon}(X_h^m(\cdot,t_{m+1};t_m),t_m)}{\triangle t},\frac{\boldsymbol{\sigma}^{\varepsilon,m+1}-\boldsymbol{\sigma}^{\varepsilon,m}}{\triangle t}\Big)\right|\\
&+\left|\Big(\frac{\boldsymbol{\sigma}^{\varepsilon,m}(\cdot)-\boldsymbol{\sigma}^{\varepsilon,m}(X(\cdot,t_{m+1};t_m))}{\triangle t},\frac{\boldsymbol{\sigma}^{\varepsilon,m+1}-\boldsymbol{\sigma}^{\varepsilon,m}}{\triangle t}\Big)\right|\\
&+\left|\Big(\frac{\boldsymbol{\sigma}^{\varepsilon,m}(X(\cdot,t_{m+1};t_m))-\boldsymbol{\sigma}^{\varepsilon,m}(X_h^m(\cdot,t_{m+1};t_m))}{\triangle t},\frac{\boldsymbol{\sigma}^{\varepsilon,m+1}-\boldsymbol{\sigma}^{\varepsilon,m}}{\triangle t}\Big)\right|\\
&+\left|\Big\langle K_{\varepsilon}(\boldsymbol{u}_{\boldsymbol{\tau}}^{\varepsilon}(\cdot,t_{m+1}))-K_{\varepsilon}(\boldsymbol{u}_{h\boldsymbol{\tau}}^{\varepsilon,m+1}),\frac{\boldsymbol{\sigma}^{\varepsilon,m+1}-\boldsymbol{\sigma}^{\varepsilon,m}}{\triangle t}\Big\rangle\right|=\sum_{i=1}^{8}II_i. \qquad (4.5)
\end{aligned}
$$

For the term $d(\frac{\boldsymbol{\sigma}^{\varepsilon,m}}{\triangle t},\zeta^{\varepsilon,m+1})$, we separate it into two cases. Let the FE subspace be $\boldsymbol{V}_h\times Q_h^0$. Then, noting that $\nabla\zeta^{\varepsilon,m+1}=0$ and using the divergence theorem, we see that

$$
\begin{aligned}
d\left(\frac{\boldsymbol{\sigma}^{\varepsilon,m}}{\triangle t},\zeta^{\varepsilon,m+1}\right)&=\frac{1}{\triangle t}\int_{\Omega}\mathrm{div}\boldsymbol{\sigma}^{\varepsilon,m}\zeta^{\varepsilon,m+1}\,\mathrm{d}x=\frac{1}{\triangle t}\sum_{K\in\mathcal{T}_h}\int_{\partial K}\zeta^{\varepsilon,m+1}\boldsymbol{\sigma}^{\varepsilon,m}\cdot\boldsymbol{n}\,\mathrm{d}s\\
&\geq-\frac{1}{\triangle t}\Big(\sum_e\int_e[\zeta^{\varepsilon,m+1}]^2\,\mathrm{d}s\Big)^{\frac12}\Big(\sum_e\int_e(\boldsymbol{\sigma}^{\varepsilon,m})^2\,\mathrm{d}s\Big)^{\frac12}\\
&\geq-\frac{1}{\triangle t}\|[\zeta^{\varepsilon,m+1}]\|_{\Gamma_h}\Big(h^{-1/2}\|\boldsymbol{\sigma}^{\varepsilon,m}\|_0+h^{1/2}\|\nabla\boldsymbol{\sigma}^{\varepsilon,m}\|_0\Big)\\
&\geq-C_1\frac{h}{\triangle t}\|[\zeta^{\varepsilon,m+1}]\|_0^2-\frac{C_2\triangle t}{h^2}\left\|\frac{\boldsymbol{\sigma}^{\varepsilon,m}}{\triangle t}\right\|_0^2,
\end{aligned}
$$

where $[\zeta^{\varepsilon,m+1}]$ denotes the jump of $\zeta^{\varepsilon,m+1}\in Q_h^0$ and $C_2=\frac{1}{4C_1}$. For the lowest equal-order FE subspace $\boldsymbol{V}_h\times Q_h^1$, in the same way, there holds

$$
\begin{aligned}
d\left(\frac{\boldsymbol{\sigma}^{\varepsilon,m}}{\triangle t},\zeta^{\varepsilon,m+1}\right)&=\frac{1}{\triangle t}\int_{\Gamma_S}\boldsymbol{\sigma}^{\varepsilon,m}\cdot\boldsymbol{n}\,\zeta^{\varepsilon,m+1}\,\mathrm{d}s-\frac{1}{\triangle t}(\boldsymbol{\sigma}^{\varepsilon,m},\nabla\zeta^{\varepsilon,m+1})\\
&\geq-\frac{C_3}{\triangle t}\|\boldsymbol{\sigma}^{\varepsilon,m}\|_0\,\|\nabla\zeta^{\varepsilon,m+1}\|_0\geq-C_4\frac{h^2}{\triangle t}\|\nabla\zeta^{\varepsilon,m+1}\|_0^2-\frac{C_5\triangle t}{h^2}\left\|\frac{\boldsymbol{\sigma}^{\varepsilon,m}}{\triangle t}\right\|_0^2,\ \left(C_5=\frac{C_3^2}{4C_4}\right).
\end{aligned}
$$

It follows from [26] that

$$
C_1\frac{h}{\triangle t}\|[\zeta^{\varepsilon,m+1}]\|_0^2\leq\frac{1}{\triangle t}\|(I-\Pi_h^1)\zeta^{\varepsilon,m+1}\|_0^2,\quad C_4\frac{h^2}{\triangle t}\|\nabla\zeta^{\varepsilon,m+1}\|_0^2\leq\frac{1}{\triangle t}\|(I-\Pi_h^0)\zeta^{\varepsilon,m+1}\|_0^2.
$$

Set the left-hand side of Eq. (4.5) be L, which can be transformed by

$$
\begin{aligned}
L\geq&\left\|\frac{\boldsymbol{\sigma}^{\varepsilon,m+1}-\boldsymbol{\sigma}^{\varepsilon,m}}{\triangle t}\right\|_0^2+\frac{\nu}{2\triangle t}(\|\nabla\boldsymbol{\sigma}^{\varepsilon,m+1}\|_0^2-\|\nabla\boldsymbol{\sigma}^{\varepsilon,m}\|_0^2)+\frac{\nu}{2}\left\|\nabla\frac{\boldsymbol{\sigma}^{\varepsilon,m+1}-\boldsymbol{\sigma}^{\varepsilon,m}}{\triangle t^{\frac12}}\right\|_0^2\\
&-\frac{C_6\triangle t}{h^2}\left\|\frac{\boldsymbol{\sigma}^{\varepsilon,m}}{\triangle t}\right\|_0^2,\ (C_6=C_2,\text{ for }\boldsymbol{V}_h\times Q_h^0\ \text{ and }\ C_6=C_5,\text{ for }\boldsymbol{V}_h\times Q_h^1).
\end{aligned}
$$

Because

$$
\begin{aligned}
\left\|\frac{\boldsymbol{\sigma}^{\varepsilon,m+1}-\boldsymbol{\sigma}^{\varepsilon,m}}{\triangle t}\right\|_0^2&=\left\|\frac{\boldsymbol{\sigma}^{\varepsilon,m+1}}{\triangle t}\right\|_0^2+\left\|\frac{\boldsymbol{\sigma}^{\varepsilon,m}}{\triangle t}\right\|_0^2-\frac{2}{\triangle t}(\boldsymbol{\sigma}^{\varepsilon,m+1},\boldsymbol{\sigma}^{\varepsilon,m})\\
&\geq(1-\triangle t)\left\|\frac{\boldsymbol{\sigma}^{\varepsilon,m+1}}{\triangle t}\right\|_0^2+(1-\triangle t)\left\|\frac{\boldsymbol{\sigma}^{\varepsilon,m}}{\triangle t}\right\|_0^2,
\end{aligned}
$$

then

$$
\begin{aligned}
L\geq&\ \frac{\nu}{2\triangle t}(\|\nabla\boldsymbol{\sigma}^{\varepsilon,m+1}\|_0^2-\|\nabla\boldsymbol{\sigma}^{\varepsilon,m}\|_0^2)+\frac12\left\|\frac{\boldsymbol{\sigma}^{\varepsilon,m+1}-\boldsymbol{\sigma}^{\varepsilon,m}}{\triangle t}\right\|_0^2+\left(\frac12(1-\triangle t)-\frac{C_6\triangle t}{h^2}\right)\left\|\frac{\boldsymbol{\sigma}^{\varepsilon,m}}{\triangle t}\right\|_0^2\\
&+\frac12(1-\triangle t)\left\|\frac{\boldsymbol{\sigma}^{\varepsilon,m+1}}{\triangle t}\right\|_0^2+\frac{\nu}{2}\left\|\nabla\frac{\boldsymbol{\sigma}^{\varepsilon,m+1}-\boldsymbol{\sigma}^{\varepsilon,m}}{\triangle t^{\frac12}}\right\|_0^2. \qquad (4.6)
\end{aligned}
$$

Since $1-\triangle t\geq0$ obviously holds and when $h^2\leq C_7-2C_6$, $\triangle t\leq\frac{C_7-2C_6}{C_7}$, $2C_6<C_7$ hold, $\frac12(1-\triangle t)-\frac{C_6}{h^2}\triangle t\geq0$ is definitely valid, then the nonnegative terms $\left(\frac12(1-\triangle t)-\frac{C_6}{h^2}\triangle t\right)\left\|\frac{\boldsymbol{\sigma}^{\varepsilon,m}}{\triangle t}\right\|_0^2$ and $\frac12(1-\triangle t)\left\|\frac{\boldsymbol{\sigma}^{\varepsilon,m+1}}{\triangle t}\right\|_0^2$ in (4.6) can be dropped.

Next we carefully explore the conditions for $\triangle t$ and h. If $\frac{1}{2}(1-\triangle t)-\frac{C_6\triangle t}{h^2}\geq 0$, we have

$$\triangle t<\frac{\triangle t}{1-\triangle t}\leq\frac{1}{2C_6}h^2.$$

So there exists a constant C_7, independent of h and $\triangle t$, when $C_7>2C_6$ as $\frac{1}{C_7}<\frac{1}{2C_6}$, such that

$$\triangle t\leq\frac{1}{C_7}h^2. \tag{4.7}$$

Then if the coefficient of term $\left\|\frac{\boldsymbol{\sigma}^{\varepsilon,m}}{\triangle t}\right\|_0^2$ is nonnegative, replacing $\triangle t$, there is,

$$\frac{1}{2}(1-\triangle t)-\frac{C_6}{h^2}\triangle t\geq\frac{1}{2}\left(1-\frac{1}{C_7}h^2\right)-\frac{C_6}{h^2}\cdot\frac{1}{C_7}h^2=\frac{C_7-2C_6}{2C_7}-\frac{1}{2C_7}h^2\geq 0,$$

thus

$$h^2\leq C_7-2C_6,$$

substituting the above estimate to (4.7) comes into

$$\triangle t\leq\frac{C_7-2C_6}{C_7}.$$

Therefore, we seek out the conditions $h^2\leq C_7-2C_6$ and $\triangle t\leq\frac{C_7-2C_6}{C_7}$ to make sure $\frac{1}{2}(1-\triangle t)-\frac{C_6}{h^2}\triangle t\geq 0$. Now (4.5) turns into

$$\frac{\nu}{2\triangle t}(\|\nabla\boldsymbol{\sigma}^{\varepsilon,m+1}\|_0^2-\|\nabla\boldsymbol{\sigma}^{\varepsilon,m}\|_0^2)+\frac{1}{2}\left\|\frac{\boldsymbol{\sigma}^{\varepsilon,m+1}-\boldsymbol{\sigma}^{\varepsilon,m}}{\triangle t}\right\|_0^2+\frac{\nu}{2}\left\|\nabla\frac{\boldsymbol{\sigma}^{\varepsilon,m+1}-\boldsymbol{\sigma}^{\varepsilon,m}}{(\triangle t)^{\frac{1}{2}}}\right\|_0^2\leq\sum_{i=1}^{8}II_i. \tag{4.8}$$

By a similar argument to that in [19], the estimates of II_i $(i=1,\ldots,7)$ are directly given as follows

$$\begin{aligned}\sum_{i=1}^{7}II_i\leq\ & \epsilon_3\left\|\frac{\boldsymbol{\sigma}^{\varepsilon,m+1}-\boldsymbol{\sigma}^{\varepsilon,m}}{\triangle t}\right\|_0^2+\frac{2\epsilon_4}{3}\left\|\nabla\frac{\boldsymbol{\sigma}^{\varepsilon,m+1}-\boldsymbol{\sigma}^{\varepsilon,m}}{\triangle t^{\frac{1}{2}}}\right\|_0^2+C\triangle t\|\mathcal{D}_t^2\boldsymbol{u}^{\varepsilon}(\cdot,t_{m+1})\|^2_{L^2(t_m,t_{m+1};\boldsymbol{Y})}\\ &+C\left(\|\boldsymbol{\phi}^{\varepsilon,m}\|_0^2+\triangle t\left\|\frac{\mathrm{d}\boldsymbol{u}^{\varepsilon}(\cdot,t_{m+1})}{\mathrm{d}t}\right\|^2_{L^2(t_m,t_{m+1};\boldsymbol{Y})}\right)+\frac{C}{\triangle t}\left\|\frac{\mathrm{d}\boldsymbol{\delta}^{\varepsilon,m+1}}{\mathrm{d}t}\right\|^2_{L^2(t_m,t_{m+1};\boldsymbol{Y})}\\ &+C\|\boldsymbol{\delta}^{\varepsilon,m+1}\|^2_{L^\infty(0,T;\boldsymbol{H}^1(\Omega))}+C(1+\frac{\alpha_m}{\triangle t})\|\boldsymbol{\delta}^{\varepsilon,m+1}\|^2_{L^\infty(0,T;\boldsymbol{H}^1(\Omega))}+C\left(1+\frac{\alpha_m}{\triangle t}\right)\|\nabla\boldsymbol{\sigma}^{\varepsilon,m}\|_0^2,\end{aligned}$$

where $\alpha_m=D_N(h)^2(\triangle t^2+\triangle t\|\frac{\mathrm{d}\boldsymbol{u}^{\varepsilon}(\cdot,m)}{\mathrm{d}t}\|^2_{L^2(t_m,t_{m+1};\boldsymbol{Y})})$ and $D_N(h)=h^{1-\frac{N}{2}}(\log\frac{1}{h})^{1-\frac{1}{N}}$.

Imitating the estimates of I_8,

$$\begin{aligned}II_8&=\left|\langle K_\varepsilon(\boldsymbol{u}_{\boldsymbol{\tau}}^{\varepsilon}(\cdot,t_{m+1}))-K_\varepsilon(\boldsymbol{u}_{h\boldsymbol{\tau}}^{\varepsilon,m+1}),\frac{\boldsymbol{\sigma}^{\varepsilon,m+1}-\boldsymbol{\sigma}^{\varepsilon,m}}{\triangle t}\rangle\right|\\ &\leq\int_{\Gamma_S}g\left|\frac{\boldsymbol{u}_{\boldsymbol{\tau}}^{\varepsilon}(\cdot,t_{m+1})}{\sqrt{|\boldsymbol{u}_{\boldsymbol{\tau}}^{\varepsilon}(\cdot,t_{m+1})|^2+\varepsilon^2}}-\frac{\boldsymbol{u}_{h\boldsymbol{\tau}}^{\varepsilon,m+1}}{\sqrt{|\boldsymbol{u}_{h\boldsymbol{\tau}}^{\varepsilon,m+1}|^2+\varepsilon^2}}\right|\cdot\left|\frac{\boldsymbol{\sigma}^{\varepsilon,m+1}-\boldsymbol{\sigma}^{\varepsilon,m}}{\triangle t}\right|\mathrm{d}s,\\ &\leq\int_{\Gamma_S}g\frac{\varepsilon^2}{(|\widetilde{\boldsymbol{u}_{h\boldsymbol{\tau}}^{\varepsilon}}(\cdot,t_{m+1})|^2+\varepsilon^2)^{3/2}}\cdot|\boldsymbol{u}_{\boldsymbol{\tau}}^{\varepsilon}(\cdot,t_{m+1})-\boldsymbol{u}_{h\boldsymbol{\tau}}^{\varepsilon,m+1}|\cdot\left|\frac{\boldsymbol{\sigma}^{\varepsilon,m+1}-\boldsymbol{\sigma}^{\varepsilon,m}}{\triangle t}\right|\mathrm{d}s\\ &\leq C\|g\|_{L^\infty(\Gamma_S)}\|\boldsymbol{\phi}^{\varepsilon,m+1}\|_{0,\Gamma_S}\left\|\frac{\boldsymbol{\sigma}^{\varepsilon,m+1}-\boldsymbol{\sigma}^{\varepsilon,m}}{\triangle t}\right\|_{0,\Gamma_S}\\ &\leq C\|\nabla\boldsymbol{\phi}^{\varepsilon,m+1}\|_0\left\|\nabla\frac{\boldsymbol{\sigma}^{\varepsilon,m+1}-\boldsymbol{\sigma}^{\varepsilon,m}}{\triangle t}\right\|_0\leq C\|\nabla\boldsymbol{\phi}^{\varepsilon,m+1}\|_0^2+\frac{\epsilon_4}{3}\left\|\nabla\frac{\boldsymbol{\sigma}^{\varepsilon,m+1}-\boldsymbol{\sigma}^{\varepsilon,m}}{(\triangle t)^{\frac{1}{2}}}\right\|_0^2.\end{aligned}$$

Using the Poincare–Friedrichs inequality $\|\boldsymbol{\phi}^m\|_0\leq C\|\nabla\boldsymbol{\phi}^m\|_0$ and substituting the estimates $\sum_{i=1}^{7}II_i$ and II_8 into Eq. (4.8), multiplying by $2\triangle t$ and summing from 0 to n for index m, then choosing $\epsilon_3=\frac{1}{2}$ and $\epsilon_4=\frac{\nu}{4}$, we obtain

$$\begin{aligned}
&\nu\|\nabla\boldsymbol{\sigma}^{\varepsilon,n+1}\|_0^2+\frac{\triangle t}{2}\sum_{m=0}^{n}\left\|\frac{\boldsymbol{\sigma}^{\varepsilon,m+1}-\boldsymbol{\sigma}^{\varepsilon,m}}{\triangle t}\right\|_0^2+\frac{\triangle t}{2}\sum_{m=0}^{n}\left\|\nabla\frac{\boldsymbol{\sigma}^{\varepsilon,m+1}-\boldsymbol{\sigma}^{\varepsilon,m}}{\triangle t^{\frac{1}{2}}}\right\|_0^2\\
&\quad\le C\triangle t^2\left(\|\mathcal{D}_t^2\boldsymbol{u}^{\varepsilon}\|_{L^2(0,T;\boldsymbol{Y})}^2+\left\|\frac{\mathrm{d}\boldsymbol{u}^{\varepsilon}}{\mathrm{d}t}\right\|_{L^2(0,T;\boldsymbol{Y})}^2\right)+C\left(1+\sum_{m=0}^{n}\alpha_m\right)\|\boldsymbol{\delta}^{\varepsilon}\|_{L^\infty(0,T;\boldsymbol{H}^1(\Omega))}^2+C\left\|\frac{\mathrm{d}\boldsymbol{\delta}^{\varepsilon}}{\mathrm{d}t}\right\|_{L^2(0,T;\boldsymbol{Y})}^2\\
&\qquad+C\triangle t\sum_{m=0}^{n+1}\|\nabla\boldsymbol{\phi}^{\varepsilon,m}\|_0^2+C\sum_{m=0}^{n}(\alpha_m+\triangle t)\|\nabla\boldsymbol{\sigma}^{\varepsilon,m}\|_0^2.
\end{aligned}$$

Since $\sum_{m=0}^{n}\alpha_m=D_N(h)^2\triangle t(T+\|\frac{\mathrm{d}\boldsymbol{u}^{\epsilon}}{\mathrm{d}t}\|_{L^2(0,T;\boldsymbol{Y})}^2)$ and $D_N(h)^2\triangle t=\mathcal{O}(1)$ as $h\to 0$, using assumption (H1) and Lemma 4 imply that

$$\begin{aligned}
\|\nabla\boldsymbol{\phi}^{\varepsilon,n+1}\|_0^2&\le 2\|\nabla\boldsymbol{\delta}^{\varepsilon,n+1}\|_0^2+2\|\nabla\boldsymbol{\sigma}^{\varepsilon,n+1}\|_0^2\\
&\le C\triangle t^2\left(\|\mathcal{D}_t^2\boldsymbol{u}^{\varepsilon}\|_{L^2(0,T;\boldsymbol{Y})}^2+\left\|\frac{\mathrm{d}\boldsymbol{u}^{\varepsilon}}{\mathrm{d}t}\right\|_{L^2(0,T;\boldsymbol{Y})}^2\right)+C\triangle t\sum_{m=0}^{n+1}\|\nabla\boldsymbol{\phi}^{\varepsilon,m}\|_0^2\\
&\quad+Ch^2\left(\|\boldsymbol{u}^{\varepsilon}\|_{L^\infty(0,T;\boldsymbol{H}^2(\Omega))}+\left\|\frac{\mathrm{d}\boldsymbol{u}^{\varepsilon}}{\mathrm{d}t}\right\|_{L^2(0,T;\boldsymbol{H}^2(\Omega))}+\|p^{\varepsilon}\|_{L^\infty(0,T;H^1(\Omega))}^2+\left\|\frac{\mathrm{d}p^{\varepsilon}}{\mathrm{d}t}\right\|_{L^2(0,T;H^1(\Omega))}^2\right).
\end{aligned}$$

A further use of Lemma 4 completes the proof.

4.2. L^2 estimate for pressure

Theorem 7. *Under assumptions (H1)–(H5), the following error estimate for the pressure holds*

$$\|p^{\varepsilon}-p_h^{\varepsilon}\|_{l^2(0,T;Q)}\le C(\triangle t+h).$$

Proof. For $\boldsymbol{v}_h\in\overset{\circ}{\boldsymbol{V}}_h$ and $q_h\in Q_h$, from the definition $\mathcal{B}_h$ and Eq. (2.5) it follows that

$$\begin{aligned}
\mathcal{B}_h((\boldsymbol{\sigma}^{\varepsilon,m},\zeta^{\varepsilon,m});(\boldsymbol{v}_h,q_h))=&\ (\mathcal{D}_t\boldsymbol{u}^{\varepsilon}(\cdot,t_{m+1})-\mathrm{d}_t\boldsymbol{u}^{\varepsilon}(\cdot,t_{m+1}),\boldsymbol{v}_h)+(\mathrm{d}_t\boldsymbol{\delta}^{\varepsilon}(\cdot,t_{m+1}),\boldsymbol{v}_h)\\
&-(\mathrm{d}_t\boldsymbol{\sigma}^{\varepsilon,m+1},\boldsymbol{v}_h).
\end{aligned}$$

From Lemma 2, we see that

$$\begin{aligned}
\beta_2(\|\nabla\boldsymbol{\sigma}^{\varepsilon,m}\|_0+\|\zeta^{\varepsilon,m}\|_0)&\le\sup_{0\neq(\boldsymbol{v}_h,q_h)\in\overset{\circ}{\boldsymbol{V}}_h\times Q_h}\frac{|\mathcal{B}_h((\boldsymbol{\sigma}^{\varepsilon,m},\zeta^{\varepsilon,m});(\boldsymbol{v}_h,q_h))|}{\|\nabla\boldsymbol{v}_h\|_0+\|q_h\|_0}\\
&=\sup_{(\boldsymbol{v}_h,q_h)\in\overset{\circ}{\boldsymbol{V}}_h\times Q_h}\frac{|(\mathcal{D}_t\boldsymbol{u}^{\varepsilon}(\cdot,t_{m+1})-\mathrm{d}_t\boldsymbol{u}^{\varepsilon}(\cdot,t_{m+1}),\boldsymbol{v}_h)+(\mathrm{d}_t\boldsymbol{\delta}^{\varepsilon}(\cdot,t_{m+1}),\boldsymbol{v}_h)-(\mathrm{d}_t\boldsymbol{\sigma}^{\varepsilon,m+1},\boldsymbol{v}_h)|}{\|\nabla\boldsymbol{v}_h\|_0+\|q_h\|_0}.
\end{aligned}$$

Furthermore, note that

$$\begin{aligned}
\|\zeta^{\varepsilon,m+1}\|_0\le&\left\|\mathcal{D}_t\boldsymbol{u}^{\varepsilon}(\cdot,t_{m+1})-\frac{\boldsymbol{u}^{\varepsilon}(\cdot,t_{m+1})-\boldsymbol{u}^{\varepsilon}(X(\cdot,t_{m+1};t_m),t_m)}{\triangle t}\right\|_0\\
&+\left\|\frac{\boldsymbol{u}^{\varepsilon}(X(\cdot,t_{m+1};t_m),t_m)-\boldsymbol{u}^{\varepsilon}(X_h^m(\cdot,t_{m+1};t_m),t_m)}{\triangle t}\right\|_0\\
&+\left\|\frac{\boldsymbol{\delta}^{\varepsilon}(\cdot,t_{m+1})-\boldsymbol{\delta}^{\varepsilon}(\cdot,t_m)}{\triangle t}\right\|_0+\left\|\frac{\boldsymbol{\delta}^{\varepsilon}(\cdot,t_m)-\boldsymbol{\delta}^{\varepsilon}(X(\cdot,t_{m+1};t_m),t_m)}{\triangle t}\right\|_{-1}\\
&+C\left\|\frac{\boldsymbol{\delta}^{\varepsilon}(X(\cdot,t_{m+1};t_m),t_m)-\boldsymbol{\delta}^{\varepsilon}(X_h^m(\cdot,t_{m+1};t_m),t_m)}{\triangle t}\right\|_{0,1}\\
&+\left\|\frac{\boldsymbol{\sigma}^{\varepsilon,m}(\cdot)-\boldsymbol{\sigma}^{\varepsilon,m}(X(\cdot,t_{m+1};t_m))}{\triangle t}\right\|_{-1}+C\left\|\frac{\boldsymbol{\sigma}^{\varepsilon,m}(X(\cdot,t_{m+1};t_m))-\boldsymbol{\sigma}^{\varepsilon,m}(X_h^m(\cdot,t_{m+1};t_m))}{\triangle t}\right\|_{0,1}\\
&+\left\|\frac{\boldsymbol{\sigma}^{\varepsilon,m+1}}{\triangle t}\right\|_0+\left\|\frac{\boldsymbol{\sigma}^{\varepsilon,m}}{\triangle t}\right\|_0,
\end{aligned}$$

and

$$\|p^{\varepsilon}-p_h^{\varepsilon}\|_{l^2(0,T;Q)}\le\ \|p^{\varepsilon}-\mathcal{Q}_h\|_{l^2(0,T;Q)}+\|\mathcal{Q}_h-p_h^{\varepsilon}\|_{l^2(0,T;Q)}.$$

Applying a similar technique as in the proof of the previous theorem, the discrete Gronwall's lemma and the results in Theorem 5, the proof can be done.

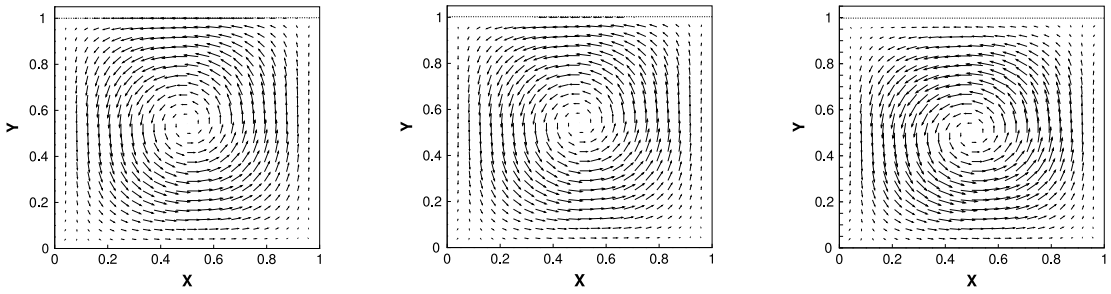

(a) $g = 0.1$. (b) $g = 0.5$. (c) $g = 1.0$.

Fig. 1. Velocity field in Ω under the lowest equal-order FE subspaces $\boldsymbol{V}_h \times Q_h^1$.

5. Numerical examples

In this part, we will assess the performances of the characteristic stabilized methods to solve the time-dependent Navier–Stokes equations with nonlinear slip boundary conditions of the friction type. Firstly, we validate the convergence properties of the proposed method to solve a test problem, slip and non-slip phenomena are observed on the boundary. Then, this method is extended to a bifurcated blood flow model, the computational domain is investigated with a stenosis or without. For the nonlinear term in scheme (3.1), the Newton iteration is applied and iterative initial value is the solution of the Stokes problem. We set the iterative tolerance as 10^{-6}, the regularization parameter $\varepsilon = 10^{-6}$ and the final time $T = 1$ unless other specified explanations are made.

5.1. A smooth problem

Let $\Omega = [0, 1]^2$ be the unit square. The boundary Γ consists of two portions Γ_D and Γ_S given by

$$\Gamma_S = \{(x, 1) \mid 0 < x < 1\}, \quad \Gamma_D = \Gamma \setminus \Gamma_S.$$

A uniform mesh partition of Ω into triangular elements is obtained by dividing Ω into sub-squares of equal size and then drawing the diagonal in each sub-square (Friedrichs–Keller type).

We consider the following exact solution $\boldsymbol{u}(x, y, t) = (u_1(x, y, t), u_2(x, y, t))$ satisfying $\boldsymbol{u}|_\Gamma = 0$:

$$\begin{cases} u_1(x, y, t) = 10x^2(x-1)^2y(y-1)(2y-1)\cos t, \\ u_2(x, y, t) = -10x(x-1)(2x-1)y^2(y-1)^2\cos t, \\ p(x, y, t) = 10(2x-1)(2y-1)\cos t. \end{cases} \tag{5.1}$$

For this test, we set $\nu = 1.0$ and $\triangle t = 0.001$ except for additional statement. The external force $\boldsymbol{f}$ is suitably obtained from (1.1). By direct computation, we have

$$\max_{\Gamma_S} |\boldsymbol{\sigma}_{\boldsymbol{\tau}}| = \max_{0 \le x \le 1} |10x^2(x-1)^2 \cos t| = 0.625 \cos t.$$

Now we impose the slip boundary on Γ_S, with g being constant, it is immediate to see that

$$\begin{cases} g \ge 0.625 \cos t \Rightarrow (5.1) \text{ remains a solution} \Rightarrow \text{ No-slip occurs.} \\ g < 0.625 \cos t \Rightarrow (5.1) \text{ is no longer a solution} \Rightarrow \text{Slip occurs.} \end{cases}$$

Such behaviors are clearly characterized by our numerical solutions in Figs. 1–2 for three different values of g with uniform grids of 24×24. In fact, slip phenomena ($\boldsymbol{u}_{h\boldsymbol{\tau}} \neq 0$) take place on Γ_S for $g = 0.1$ and $g = 0.5$, whereas non-slip phenomena are observed for $g = 1.0$, where we omit $\cos T$ in g since the results are selected at the final time in all the numerical examples. It is shown that the bigger the threshold function g, the more difficult it becomes for a non-trivial slip to occur.

We now display the relative errors $E_{L^2}(p)$, $E_{H^1}(\boldsymbol{u})$, and $E_{L^2}(\boldsymbol{u})$ in Tables 1–4 when g changes, where

$$E_{L^2}(p) = \frac{\|p - p_h^\varepsilon\|_0}{\|p\|_0}, \; E_{H^1}(\boldsymbol{u}) = \frac{\|\nabla(\boldsymbol{u} - \boldsymbol{u}_h^\varepsilon)\|_0}{\|\nabla \boldsymbol{u}\|_0}, \; E_{L^2}(\boldsymbol{u}) = \frac{\|\boldsymbol{u} - \boldsymbol{u}_h^\varepsilon\|_0}{\|\boldsymbol{u}\|_0}.$$

Since the explicit solution is unknown when $g = 0.5$, we regard the approximate solution with grids of 120×120 as a reference solution $(\boldsymbol{u}_{ref}, p_{ref})$. However, we know the exact solution (5.1) when $g = 1.0$ and thus we take $\boldsymbol{u}_{ref} = \boldsymbol{u}$, $p_{ref} = p$. The convergence rates depending on the time size is characterized in Table 5 with a fixed mesh size $h = 1/50$. Fig. 3–4 displayed the convergence behaviors under different Reynolds numbers: 1, 400, 1000, where I stands for the FE subspace $\boldsymbol{V}_h \times Q_h^0$ and J for the FE subspace $\boldsymbol{V}_h \times Q_h^1$. From the gained results, we observe that the spacial optimal convergence-order $\mathcal{O}(h)$ for the H^1-norm of velocity, L^2-norm of pressure and $\mathcal{O}(h^2)$ for the L^2-norm of velocity, along with the convergence rate $\mathcal{O}(\triangle t)$ depends the time size, which are consistent with the theoretical analysis in Section 4.

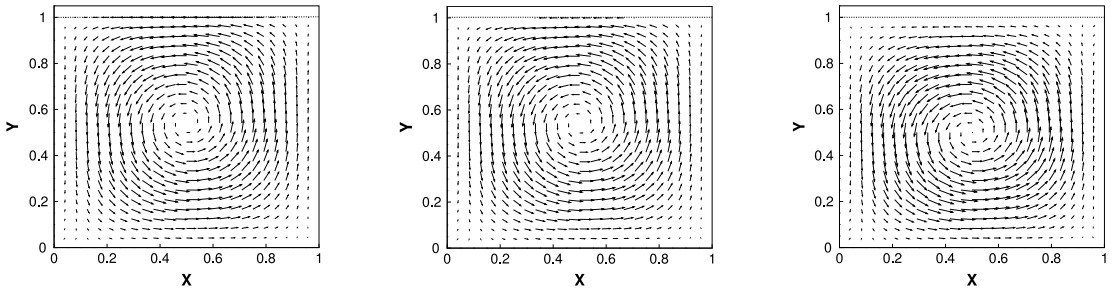

(a) $g = 0.1$. (b) $g = 0.5$. (c) $g = 1.0$.

Fig. 2. Velocity field in Ω under the lowest order FE subspaces $\boldsymbol{V}_h \times Q_h^0$.

Table 1
Convergence behavior of $\|\boldsymbol{u}_h - \boldsymbol{u}_{ref}\|$ and $\|p_h - p_{ref}\|$ for $g = 0.5$.

$\frac{1}{h}$	$\boldsymbol{V}_h \times Q_h^1$ FE subspace					
	$E_{L^2}(p)$	Rate	$E_{H^1}(\boldsymbol{u})$	Rate	$E_{L^2}(\boldsymbol{u})$	Rate
8	1.706E−1	–	5.177E−1	–	3.690E−1	–
16	7.765E−2	1.14	2.106E−1	1.30	9.678E−2	1.93
24	4.927E−2	1.12	1.2653-1	1.26	4.279E−2	2.01
32	3.819E−2	0.89	9.419E−2	1.03	2.348E−2	2.09
40	2.785E−2	1.42	6.808E−2	1.45	1.445E−2	2.08

Table 2
Convergence behavior of $\|\boldsymbol{u}_h - \boldsymbol{u}_{ref}\|$ and $\|p_h - p_{ref}\|$ for $g = 0.5$.

$\frac{1}{h}$	$\boldsymbol{V}_h \times Q_h^0$ FE subspace					
	$E_{L^2}(p)$	Rate	$E_{H^1}(\boldsymbol{u})$	Rate	$E_{L^2}(\boldsymbol{u})$	Rate
8	9.906E−2	–	5.538E−1	–	3.715E−1	–
16	3.007E−2	1.72	2.207E−2	1.33	9.460E−2	1.97
24	1.483E−2	1.74	1.314E−1	1.28	4.151E−2	2.03
32	8.893E−3	1.78	9.696E−2	1.06	2.270E−2	2.09
40	5.912E−3	1.83	6.997E−2	1.46	1.395E−2	2.18

Table 3
Convergence behavior of $\|\boldsymbol{u} - \boldsymbol{u}_h\|$ and $\|p - p_h\|$ for $g = 1.0$.

$\frac{1}{h}$	$\boldsymbol{V}_h \times Q_h^1$ FE subspace					
	$E_{L^2}(p)$	Rate	$E_{H^1}(\boldsymbol{u})$	Rate	$E_{L^2}(\boldsymbol{u})$	Rate
8	1.195E−1	–	6.333E−1	–	4.210E−1	–
16	3.590E−2	1.73	2.501E−1	1.34	1.143E−1	1.88
24	1.775E−2	1.74	1.494E−1	1.27	5.208E−2	1.94
32	1.079E−2	1.73	1.054E−1	1.21	2.978E−2	1.94
40	7.353E−3	1.72	8.118E−2	1.17	1.911E−2	1.99

Table 4
Convergence behavior of $\|\boldsymbol{u} - \boldsymbol{u}_h\|$ and $\|p - p_h\|$ for $g = 1.0$.

$\frac{1}{h}$	$\boldsymbol{V}_h \times Q_h^0$ FE subspace					
	$E_{L^2}(p)$	Rate	$E_{H^1}(\boldsymbol{u})$	Rate	$E_{L^2}(\boldsymbol{u})$	Rate
8	1.834E−1	–	5.942E−1	–	4.130E−1	–
16	8.000E−2	1.20	2.388E−1	1.31	1.154E−1	1.84
24	5.113E−2	1.10	1.440E−1	1.25	5.307E−2	1.92
32	3.764E−2	1.06	1.022E−1	1.19	3.049E−2	1.93
40	2.981E−2	1.04	7.905E−2	1.15	1.958E−2	1.99

5.2. Numerical simulation of a bifurcated blood flow model

This example studies a two-dimensional simplified model of hemokinesis in a bifurcated arterial vessel whose main vessel wall may have an arterial stenosis, as shown in Fig. 5 [34,35]. Assume that the blood vessel acts as a "Y"-glyph pipe with a certain length, Fig. 5(b) attached with a half-square stenosis on the wall of the main vessel. Blood flows into the vessel

Table 5
Relative errors and convergence rates of different time size when $g = 1.0$.

$\triangle t$	$\boldsymbol{V}_h \times Q_h^1$				$\boldsymbol{V}_h \times Q_h^0$			
	$E_{L^2}(\boldsymbol{u})$	Rate	$E_{H^1}(\boldsymbol{u})$	Rate	$E_{L^2}(\boldsymbol{u})$	Rate	$E_{H^1}(\boldsymbol{u})$	Rate
0.5	9.89809	–	9.87599	–	9.93787	–	9.93783	–
0.1	2.07197	0.972	2.07774	0.969	2.26594	0.915	2.26803	0.918
0.05	1.04083	0.993	1.06203	0.968	1.18563	0.935	1.21138	0.936
0.01	0.209027	0.997	0.234829	0.938	0.251769	0.963	0.267785	0.925

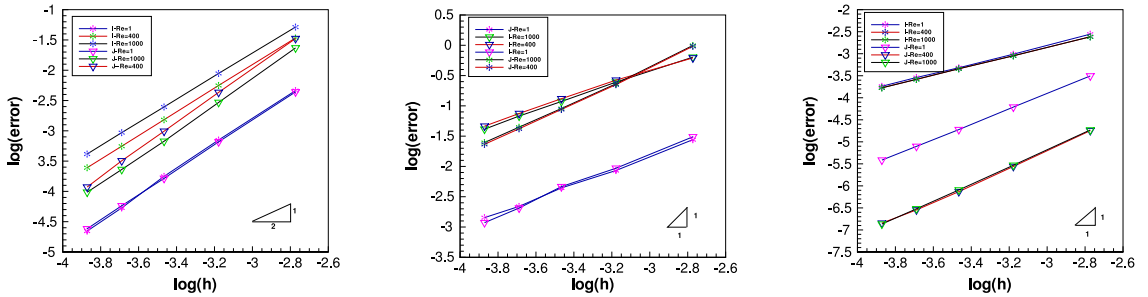

(a) L^2 convergence order for velocity. (b) H^1 convergence order for velocity. (c) L^2 convergence order for pressure.

Fig. 3. Convergence orders under different Reynolds numbers with $\triangle t = h^2$ when $g = 0.1$.

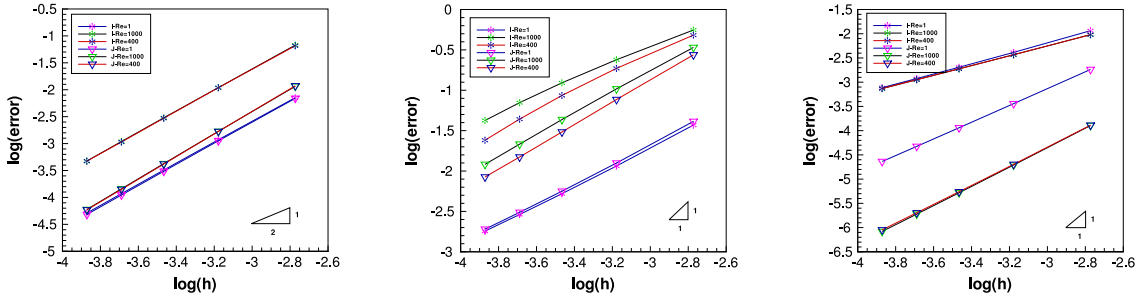

(a) L^2 convergence order for velocity. (b) H^1 convergence order for velocity. (c) L^2 convergence order for pressure.

Fig. 4. Convergence orders under different Reynolds numbers with $\triangle t = h^2$ when $g = 1.0$.

(a) Without stenosis. (b) With stenosis.

Fig. 5. Calculation region of the bifurcation vascular model.

from the left entrance and two outlets are labeled. The top and bottom boundaries drawn in dashed lines in the main vessel can be chosen as a Dirichlet or slip boundary, the rest of the regional boundaries is imposed with a Dirichlet boundary. Set the diameter of the main vessel as 2, the width of the main branch outlet as 1.25, and that of the other branch as 0.75. The specific ratio between the width of the stenosis and the diameter of the main vessel is used to describe the degree of arterial stenosis, noted by S.

For the grid generation, 40 grid points are scattered on per unit length and Delaunay mesh generation method is applied (Fig. 6 displays the mesh generation and 5 points are scattered on per unit length just for intuitive exhibition, refined mesh is employed on the singular points for Fig. 6(b)). The inflow velocities are: $u_x = 1.2 - 1.2(y-1)^2$, $u_y = 0$, $u_{0x} = 1.2$, and

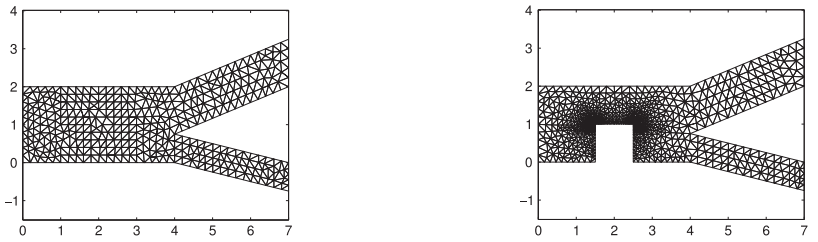

(a) Without stenosis. (b) With stenosis.

Fig. 6. Calculation region of the bifurcation vascular model.

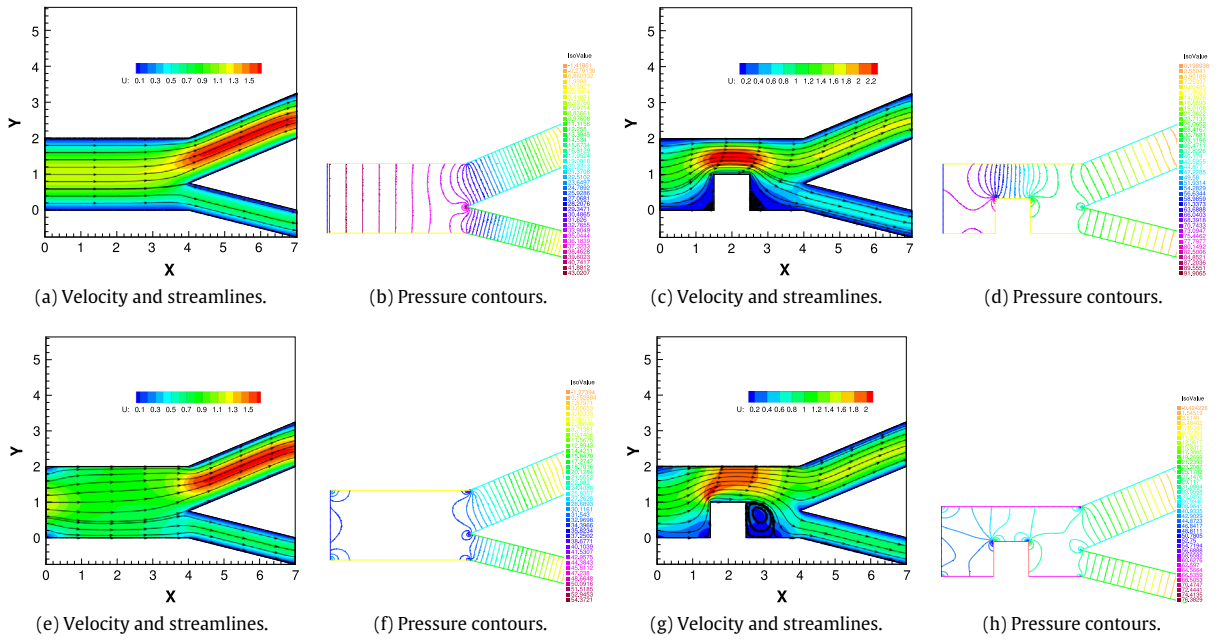

(a) Velocity and streamlines. (b) Pressure contours. (c) Velocity and streamlines. (d) Pressure contours.

(e) Velocity and streamlines. (f) Pressure contours. (g) Velocity and streamlines. (h) Pressure contours.

Fig. 7. The velocity and streamlines, pressure contours of blood flow with different boundary conditions: Dirichlet (a–d) and slip (e–h) under finite subspace $\boldsymbol{V}_h \times Q_h^1$.

$u_{0y} = 0$; the viscosity coefficient $\nu = 1.0$, and we set the time size $\triangle t = h^2$, the frictional function $g = |\nu \frac{\partial \boldsymbol{u}_{h\tau}}{\partial \boldsymbol{n}}|$ when the slip boundary is considered. Fig. 7, 8 show the values of velocity, streamlines and pressure contours at the final time with different computational domain, different boundary conditions, as well as different FE subspaces. The results of velocity and pressure are displayed in Fig. 9 when S changes, the shear stress along the bottom boundary with different S is drawn in Fig. 10, and in both Figs. 9 and 10 only slip boundary conditions are considered.

By comparing the pressure contours in Figs. 7–9, when there are no stenoses, the values of the pressure change slightly in the main vessel, except the bifurcate junctions, where exists sharp change of the pressure. The values of pressure with slip boundary conditions are less than those without. When the stenoses emerge, the pressure changes rapidly around the beginning and end of the stenosis areas in the main vessel, bifurcation junctions and branches.

From the velocity figures (a), (e) and (c), (g) in Fig. 7–8, the streamlines directly flow from inlet to outlet and calculated values of velocity on the boundary are zeros when all Dirichlet boundaries are considered in the main vessel, while as the slip boundaries exist, the values of velocity on the top and bottom boundaries are non-vanishing ((a), (e)). When the stenosis exists, flow separated regions appear and form low velocity areas, and if all Dirichlet boundary conditions are considered, eddies arise at the forward and backward of the stenosis ((c) in Figs. 7–9), however, when the top and bottom boundaries are chosen as slip, eddies arise only at the backward ((g) in Figs. 7–9). As the width of the stenosis becomes larger, the separation areas enlarge, which cause the bigger local eddies ((c), (g) in Figs. 7–9).

From Fig. 10, the positions and sizes of the stenosis are easy to find, the shear stress at the beginning and end of the stenosis changes strikingly. In the low speed sections of the blood vessels, the blood platelets and fibrinogen more easily deposit, while the lower shear stress in the separation area makes the accumulation of material around the vessel walls hardly be carried off by the flowing blood, which can easily lead to vascular lesions, and then come into atherosclerosis.

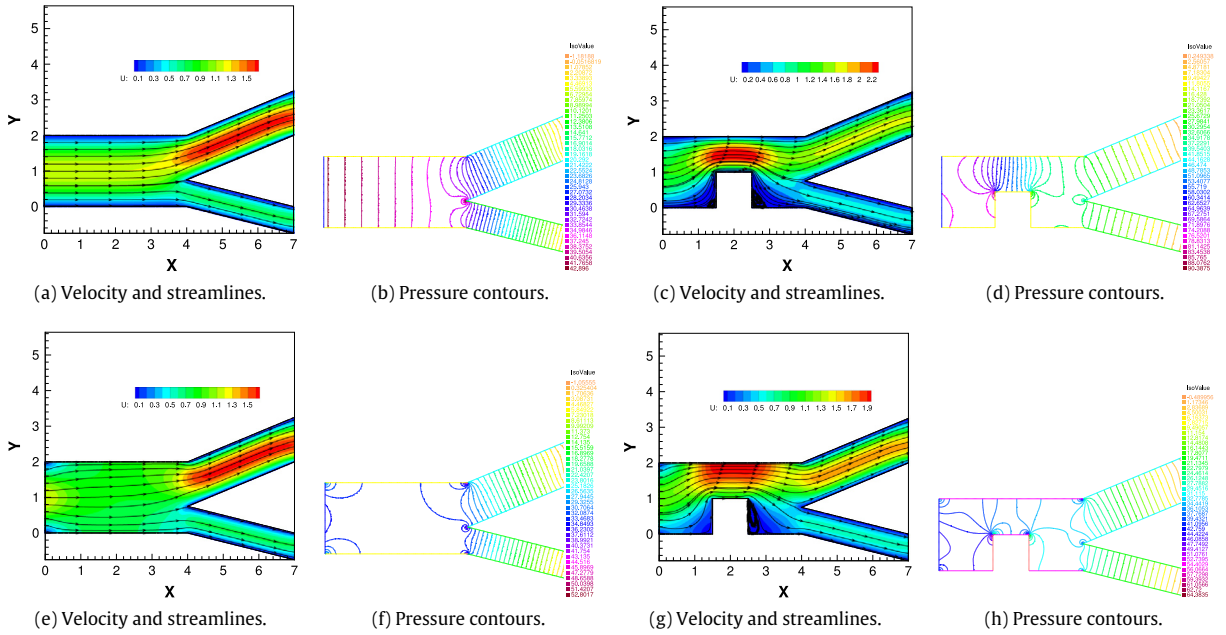

(a) Velocity and streamlines. (b) Pressure contours. (c) Velocity and streamlines. (d) Pressure contours.

(e) Velocity and streamlines. (f) Pressure contours. (g) Velocity and streamlines. (h) Pressure contours.

Fig. 8. The velocity and streamlines, pressure contours of blood flow with different boundary conditions: Dirichlet (a–d) and slip (e–h) under finite subspace $\boldsymbol{V}_h \times Q_h^0$.

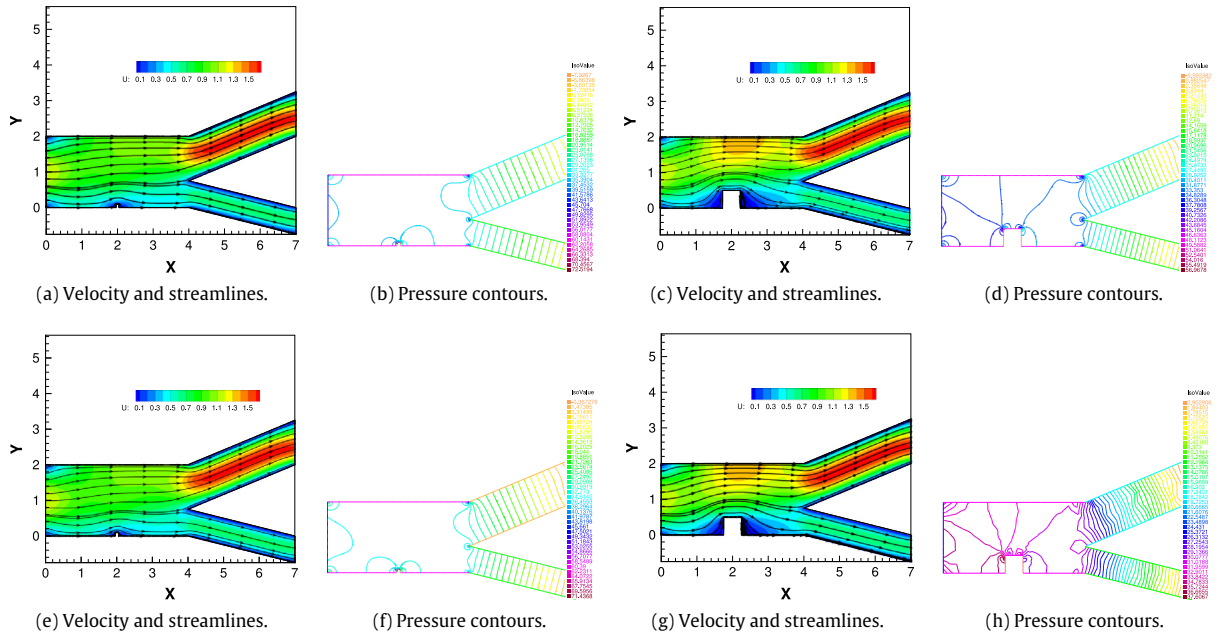

(a) Velocity and streamlines. (b) Pressure contours. (c) Velocity and streamlines. (d) Pressure contours.

(e) Velocity and streamlines. (f) Pressure contours. (g) Velocity and streamlines. (h) Pressure contours.

Fig. 9. The velocity and streamlines, pressure contours of blood flow with slip boundary conditions when $S = 0.05, 0.25$ under FE subspaces $\boldsymbol{V}_h \times Q_h^1$ (a–d) and $\boldsymbol{V}_h \times Q_h^0$ (e–h).

6. Conclusions

In this work, a characteristic finite element scheme is studied for the time-dependent Navier–Stokes equations with nonlinear slip boundary conditions. Because this type of boundary conditions includes a subdifferential property, the continuous problem is formulated as a variational inequality. By means of a regularized problem, the inequality problem

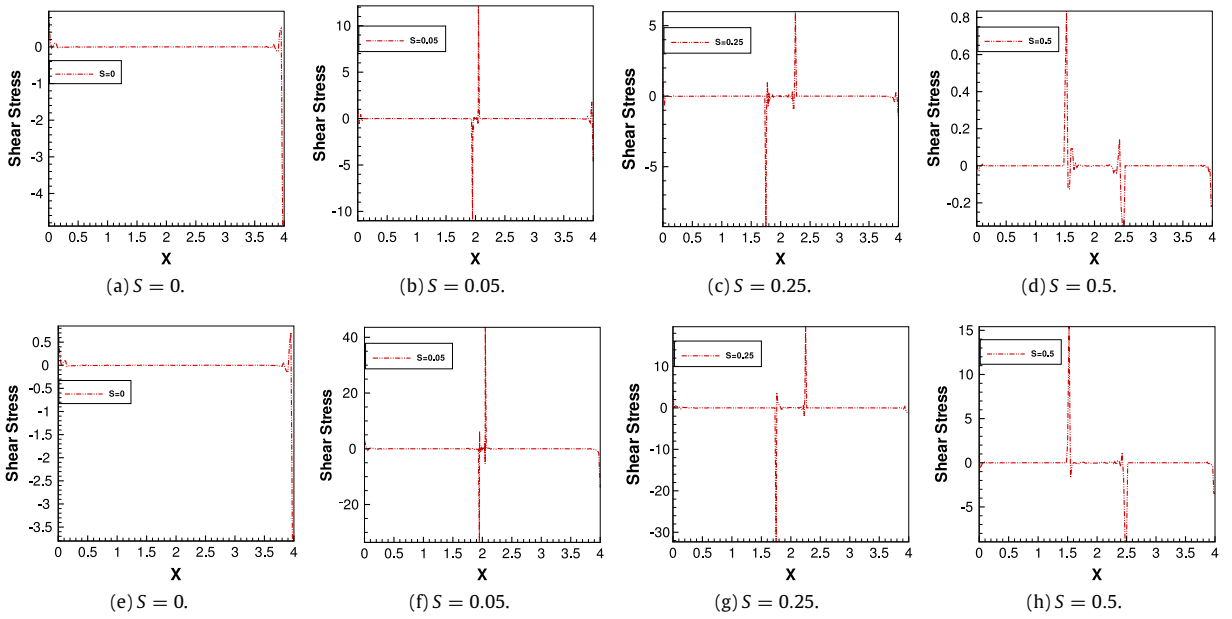

(a) $S = 0$. (b) $S = 0.05$. (c) $S = 0.25$. (d) $S = 0.5$.

(e) $S = 0$. (f) $S = 0.05$. (g) $S = 0.25$. (h) $S = 0.5$.

Fig. 10. The shear stress along the bottom boundary with different S under FE subspaces $\boldsymbol{V}_h \times Q_h^1$ (a–d) and $\boldsymbol{V}_h \times Q_h^0$ (e–h).

turns into equations and the lower finite element subspaces are chosen for the fully discrete characteristic scheme based on the pressure projection. We have proved the unconditional stability of the proposed scheme and established the optimal convergence orders for appropriately smooth solutions. Finally, numerical results verified the theoretical analysis, and illustrated the presented characteristic method exhibits good stability behavior with the nonlinear slip boundary of friction type.

References

[1] H. Fujita, Flow Problems with Unilateral Boundary Conditions, Lecons, College de France, 1993.
[2] H. Fujita, A mathematical analysis of motions of viscous incompressible fluid under leak or slip boundary conditions, RIMS Kokyuroku 888 (1994) 199–216.
[3] H. Fujita, H. Kawarada, Variational inequalities for the Stokes equation with boundary conditions of friction type, Int. Ser. Math. Sci. Appl. 11 (1998) 15–33.
[4] H. Fujita, A coherent analysis of Stokes flows under boundary conditions of friction type, J. Comput. Appl. Math. 149 (1) (2002) 57–69.
[5] N. Saito, H. Fujita, Regularity of solutions to the Stokes equation under a certain nonlinear boundary condition, Lect. Notes Pure Appl. Math. 223 (2002) 73–86.
[6] N. Saito, On the Stokes equations with the leak and slip boundary conditions of friction type: regularity of solutions, Pub RIMS, Kyoto University 40 (2) (2004) 345–383.
[7] J. Li, Y.P. Lin, H.B. Zheng, Q.S. Zou, A priori and posteriori estimates of stabilized fems for the incompressible flow with slip boundary conditions, J. Sci. Comput., revised.
[8] T. Kashiwabara, On a finite element approximation of the Stokes equations under a slip boundary condition of the friction type, J. Indust. Appl. Math. 30 (1) (2013) 227–261.
[9] Y. Li, K.T. Li, Pressure projection stabilized finite element method for Stokes problem with nonlinear slip boundary conditions, J. Comput. Appl. Math. 235 (12) (2011) 3673–3682.
[10] Y. Li, K.T. Li, Pressure projection stabilized finite element method for Navier–Stokes equations with nonlinear slip boundary conditions, Computing 87 (3–4) (2010) 113–133.
[11] X.X. Dai, P.P. Tang, M.H. Wu, Analysis of an iterative penalty method for Navier–Stokes equations with nonlinear slip boundary conditions, Internat. J. Numer. Methods Fluids 72 (4) (2013) 403–413.
[12] F.F. Jing, J. Li, Z. Chen, Stabilized finite element methods for a blood flow model of arteriosclerosis, Numer. Methods Partial Differential Equations 31 (6) (2015) 2063–2079.
[13] J.K. Djoko, On the time approximation of the Stokes equations with slip boundary condition, Int. J. Numer. Anal. Model. 11 (1) (2014) 34–53.
[14] T. Kashiwabara, On a strong solution of the non-stationary Navier–Stokes equations under slip or leak boundary conditions of friction type, J. Differential Equations 254 (2) (2013) 756–778.
[15] Y. Li, K.T. Li, Global strong solutions of two-dimensional Navier–Stokes equations with nonlinear slip boundary conditions, J. Math. Anal. Appl. 393 (1) (2012) 1–13.
[16] Y. Li, R. An, Semi-discrete stabilized finite element methods for Navier–Stokes equations with nonlinear slip boundary conditions based on regularization procedure, Numer. Math. 117 (1) (2011) 1–36.
[17] Y.N. He, J. Li, Convergence of three iterative methods based on the finite element discretization for the stationary Navier–Stokes equations, Comput. Methods Appl. Mech. Engrg. 198 (15–16) (2009) 1351–1359.

[18] J. Li, Z. Chen, Optimal L^2 H^1 and L^∞ analysis of finite volume methods for the stationary Navier–Stokes equations with large data, Numer. Math. 126 (1) (2014) 75–101.
[19] E. Suli, Convergence and nonlinear stability of the Lagrange–Galerkin method for the Navier–Stokes equations, Numer. Math. 53 (4) (1998) 459–483.
[20] J. Douglas, Jr., Thomas F. Russell, Numerical method for converction-dominated diffusion problem based on combining the method of characteristics with finite element of finite difference procedures, SIAM J. Numer. Anal. 19 (5) (1982) 871–885.
[21] K. Morton, A. Priestley, E. Suli, Convergence Analysis of the Lagrange–Galerkin Method with Non-Exact Integration, Oxford University Computing Laboratory Report, 1986.
[22] Z. Chen, Characteristic mixed discontinuous finite element methods for advection-dominated diffusion problems, Comput. Methods Appl. Mech. Engrg. 191 (23–24) (2002) 2509–2538.
[23] R.A. Adams, Sobolev Spaces, Academic Press, New York, 1975.
[24] Y. Achdou, J.L. Guermond, Analysis of a finite element projection/Lagrange–Galerkin method for the incompressible Navier–Stokes equations, SIAM J. Numer. Anal. 37 (3) (2000) 799–826.
[25] Z. Chen, Finite Element Methods and their Applications, Springer-Verlag, Heidelberg and New York, 2005.
[26] P.B. Bochev, C.R. Dohrmann, M.D. Gunzburger, Stabilization of low-order mixed finite elements for the Stokes equations, SIAM J. Numer. Anal. 44 (1) (2006) 82–101.
[27] P.G. Ciarlet, The Finte Element Method for Elliptic Problem, North-Holland, Amsterdam, 1978.
[28] J. Li, Y.N. He, A stabilized finite element method based on two local Gauss integrations for the Stokes equations, J. Comput. Appl. Math. 214 (1) (2008) 58–65.
[29] J. Li, Z. Chen, A new stabilized finite volume method for the stationary Stokes equations, Adv. Comput. Math. 30 (2) (2009) 141–152.
[30] J. Li, Y.N. He, Z. Chen, A new stabilized finite element method for the transient Navier–Stokes equations, Comput. Methods Appl. Mech. Engrg. 197 (1–4) (2007) 22–35.
[31] O. Pironneau, On the transport-diffusion algorithm and its application to the Navier–Stokes equations, Numer. Math. 38 (3) (1982) 309–332.
[32] H.E. Jia, K.T. Li, S.H. Liu, Characteristic stabilized finite element method for the transient Navier–Stokes equations, Comput. Methods Appl. Mech. Engrg. 199 (45–48) (2010) 2996–3004.
[33] V. Girault, P. Raviart, Finite Element Method for Navier–Stokes Equations: Theory and Algorithms, Springer-Verlag, Berlin, Heidelberg, 1986.
[34] L.Q. Mei, K. Zhao, The influence of arterial stenosis in bifurcate blood vessel on the blood flow, Chin. J. Appl. Mech. 30 (3) (2013) 417–421.
[35] A.K. Politis, G.P. Stavropoulos, M.N. Christolis, et al., Numerical modeling of simulated blood in idealized composite arterial coronary grafts: steady state simulations, J. Biomech. 40 (5) (2007) 1125–1136.